Geometry of Spaces of Planar Quadrilaterals

Jessica L. StClair

Dissertation submitted to the Faculty of the

Virginia Polytechnic Institute and State University

in partial fulfillment of the requirements for the degree of

Doctor of Philosophy

in

Mathematics

Peter Haskell, Chair

Martin Day

William Floyd

James Thomson

April 14, 2011

Blacksburg, Virginia

Keywords: Differential Geometry, Pre-Moduli Space, Moduli Space, Riemannian Metric,

Robotics, Holonomy

Geometry of Spaces of Planar Quadrilaterals

Jessica L. StClair

(ABSTRACT)

The purpose of this dissertation is to investigate the geometry of spaces of planar quadrilaterals. The topology of moduli spaces of planar quadrilaterals (the set of all distinct planar quadrilaterals with fixed side lengths) has been well-studied [5], [8], [10]. The symplectic geometry of these spaces has been studied by Kapovich and Millson [6], but the Riemannian geometry of these spaces has not been thoroughly examined. We study paths in the moduli space and the pre-moduli space. We compare intraplanar paths between points in the moduli space to extraplanar paths between those same points. We give conditions on side lengths to guarantee that intraplanar motion is shorter between some points. Direct applications of this result could be applied to motion-planning of a robot arm. We show that horizontal lifts to the pre-moduli space of paths in the moduli space can exhibit holonomy. We determine exactly which collections of side lengths allow holonomy.

Contents

List of Figures

Chapter 1

Introduction

Suppose we are given a prescribed ordered set of n side lengths for a polygon, where $n \geq 3$. We are interested in the set of all possible shapes that can be drawn in the plane with those side lengths. We consider two polygons equivalent if a translation and/or rotation can move one to rest on top of the other. The set of all equivalence classes, once it is given a natural topology, is called the moduli space. Because the equivalence relation is generated by translations and rotations, we may view the moduli space as parametrizing the collection of distinct shapes formed by polygons with the specified side lengths.

To visualize the moduli space we may fix one endpoint at the origin and one side along the positive x-axis. The position of the other sides determines the shape of the polygon. If we view the sides as vectors and fix one of them, we are interested in the set of all such collections of vectors having prescribed lengths and summing to zero.

If we do not fix one vector and view two polygons that differ by a rigid rotation as different shapes, the set of all such shapes is called the pre-moduli space. The pre-moduli space is the set of all collections of vectors having prescribed side lengths and summing to zero. The moduli space is then simply the quotient of the pre-moduli space by the natural $SO(2)$-action. Definitions and basic properties of the moduli space and pre-moduli space are discussed in Chapter 2.

In this dissertation we focus specifically on the case $n = 4$, quadrilaterals in the plane. In Chapter 3 we review the topology of these moduli spaces, which is well-studied, and give some original proofs of known results. The geometry of these spaces is not well-studied, and that is our focus for the remainder of the paper.

In Chapter 4 we examine the geometry of the moduli space in a way motivated by a robot arm application. We view the first three sides of a quadrilateral as segments of a robot arm with its end fixed some positive distance away from the base. We assign an appropriate notion of distance, compare motion of this arm moving in the plane to motion of the arm out of the plane, and give conditions for when it is shorter to move within the plane.

The distance used in Chapter 4 depends on the side lengths chosen and the specified order of the sides. A permutation of the side order defines a homeomorphism of the moduli spaces. In Chapter 5 we introduce a notion of distance that is independent of the chosen side order. This notion of distance comes from a Riemannian metric on the pre-moduli space. This metric is a restriction of the metric used by Kendall [7]. This metric is the foundation for a relationship between the geometry of the pre-moduli space and the geometry of the moduli

space. We study this relationship in Chapter 5.

We take a path in the moduli space, define its horizontal lift to the pre-moduli space, and examine what happens to the lifted path. In particular we give conditions on side lengths that guarantee the horizontal lift returns to its starting point. We also give conditions on side lengths that guarantee the horizontal lift does not return to its starting point. The latter phenomenon is called holonomy [4].

Chapter 2

Spaces of Planar Polygons

Let $n \geq 3$ and suppose we are given a vector of n positive side lengths, $\vec{\ell} = (\ell_1, \ldots, \ell_n)$, for an n-gon in $\mathbb{R}^2$. Let $\mathbf{x}_i = (x_i, y_i) \in \mathbb{R}^2$ be the vector of length ℓ_i that forms side i of the n-gon, for $i = 1, \ldots, n$. We assume that the longest side is less than or equal to the sum of the other sides. This ensures that at least one n-gon can be drawn in $\mathbb{R}^2$ with those side lengths. We relax our definition of polygon to allow sides to intersect at points other than the endpoints.

2.1 The Pre-Moduli Space And Moduli Space

Definition 2.1.1. We define the *pre-moduli space* of $\vec{\ell} = (\ell_1, \ldots, \ell_n)$ to be

$$\mathcal{PM}(\vec{\ell}, n) = \left\{ (\mathbf{x}_1, \ldots, \mathbf{x}_n) \in \mathbb{R}^{2n} : \|\mathbf{x}_i\| = \ell_i \text{ for all } i, \text{ and } \sum_{i=1}^{n} \mathbf{x}_i = \mathbf{0} \right\}$$

Note that the pre-moduli space is the solution set of a system of $n+2$ equations determined by smooth functions in $2n$ variables:

$$\begin{aligned} x_1^2 + y_1^2 &= \ell_1^2 \\ &\vdots \quad\quad \vdots \\ x_n^2 + y_n^2 &= \ell_n^2 \\ x_1 + \cdots + x_n &= 0 \\ y_1 + \cdots + y_n &= 0 \end{aligned}$$

We will implicitly identify $\mathbb{R}^2$ and $\mathbb{C}$, with notation $\mathbb{C}^*$ preferred when the origin is removed. Observe that, because each $\ell_i > 0$, each $\mathbf{x}_i \in \mathbb{C}^*$. Thus

$$\mathcal{PM}(\vec{\ell}, n) \subset \underbrace{\mathbb{C}^* \times \cdots \times \mathbb{C}^*}_{n \text{ times}}$$

The space $\mathbb{C}^* \times \cdots \times \mathbb{C}^*$ has a natural topology and a natural smooth structure. The pre-moduli space gets the topology induced from the ambient space. Additionally, the pre-moduli space gets a smooth structure from the ambient space at the points where its defining equations satisfy the hypotheses of the Implicit Mapping Theorem. These points occur

wherever the matrix:

$$M = \begin{bmatrix} 2x_1 & 2y_1 & 0 & 0 & \cdots & & & 0 \\ 0 & 0 & 2x_2 & 2y_2 & 0 & \cdots & & 0 \\ \vdots & & & \ddots & & & & \vdots \\ 0 & \cdots & & & & & 2x_n & 2y_n \\ 1 & 0 & 1 & 0 & \cdots & & 1 & 0 \\ 0 & 1 & 0 & 1 & \cdots & & 0 & 1 \end{bmatrix}$$

has full rank.

For $i = 1, \ldots, n, n+1, n+2$, let $\mathbf{r}_i$ be the vector representing row i of matrix M:

$$M = \begin{bmatrix} \mathbf{r}_1 \\ \mathbf{r}_2 \\ \vdots \\ \mathbf{r}_n \\ \mathbf{r}_{n+1} \\ \mathbf{r}_{n+2} \end{bmatrix}$$

Then M loses full rank if and only if

$$\sum_{i=1}^{n} c_i \mathbf{r}_i + a\mathbf{r}_{n+1} + b\mathbf{r}_{n+2} = \mathbf{0}$$

for some $c_1, \ldots, c_n, a, b$ not all zero.

By observing the placement of the zeros in the matrix, M loses full rank if and only if

$$\begin{aligned} 2c_1\mathbf{x}_1 + (a,b) &= (0,0) \\ \vdots &= \vdots \\ 2c_n\mathbf{x}_n + (a,b) &= (0,0) \end{aligned}$$

for some $c_1, \ldots, c_n, a, b$ not all zero. If $a = b = 0$, then $c_i = 0$ for all i because $\mathbf{x}_i$ is never the zero vector. Thus $(a,b) \neq (0,0)$ and hence $c_i \neq 0$ for all i.

Thus M loses full rank if and only if $\mathbf{x}_i = -\dfrac{1}{2c_i}(a,b)$ for all i, for some choices of a, b, and $c_1, \ldots, c_n$ not all zero. That is, M loses full rank if and only if all the $\mathbf{x}_i$ are collinear.

Definition 2.1.2. We define a *degenerate n-gon* to be a polygon where all the sides are collinear.

Note that a degenerate n-gon can occur if and only if $\ell_n = e_1\ell_1 + \cdots + e_n\ell_{n-1}$ for some choices of e_i, where $e_i \in \{1, -1\}$. Sometimes we will refer to these special n-gons as *straight-line configurations*. By the Implicit Mapping Theorem, the pre-moduli space is a smooth $(n-2)-$manifold everywhere but at the straight-line configurations.

Definition 2.1.3. We define the *moduli space* of $\vec{\ell} = (\ell_1, \ldots, \ell_n)$ to be

$$\mathcal{M}(\vec{\ell}, n) = \mathcal{PM}(\vec{\ell}, n)/SO(2)$$

where $SO(2)$ acts diagonally by its natural action on $\mathbb{R}^2$ on every factor.

The moduli space $\mathcal{M}(\vec{\ell}, n)$ identifies shapes in the pre-moduli space that differ by a rigid

rotation of all the vector sides. In some sense the moduli space is the set of all "distinct shapes" that can be drawn in the plane with side lengths $\vec{\ell}$.

Let $\pi : \mathcal{PM}(\vec{\ell}, n) \longrightarrow \mathcal{M}(\vec{\ell}, n)$ be the quotient map. Then the moduli space gets the quotient topology. In fact, because $SO(2)$ acts freely on $\mathcal{PM}(\vec{\ell}, n)$, it is a consequence of the slice theorem for actions of compact Lie groups (see, e.g., [1]) that the quotient $\mathcal{M}(\vec{\ell}, n)$ is a smooth $(n-3)$-manifold everywhere but at the straight-line configurations. We provide no further details here because we do not use this result anywhere in this paper.

The pre-moduli space allows the last side to point in any direction. We wish to fix the last side and use that as a representation of $\mathcal{M}(\vec{\ell}, n)$.

Lemma 2.1.4. *There exists a map $H : \mathcal{M}(\vec{\ell}, n) \longrightarrow \mathcal{PM}(\vec{\ell}, n)$ such that $\pi(H(w)) = w$ for all $w \in \mathcal{M}(\vec{\ell}, n)$.*

Proof. A formal proof can be found in Appendix A. This lemma says that H is a section. □

A consequence of Lemma 2.1.4 is that $\mathcal{PM}(\vec{\ell}, n)$ has a natural product structure:

Proposition 2.1.5.

$$\mathcal{PM}(\vec{\ell}, n) = \mathcal{M}(\vec{\ell}, n) \times \mathcal{S}^1.$$

For convenience we choose to fix ℓ_n along the positive x-axis. Then the moduli space may also be defined as

$$\mathcal{M}(\vec{\ell}, n) = \left\{ (\mathbf{x}_1, \ldots, \mathbf{x}_n) \in \mathbb{R}^{2n} : \|\mathbf{x}_i\| = \ell_i, \sum_{i=1}^{n} \mathbf{x}_i = \mathbf{0}, \mathbf{x}_n = (-\ell_n, 0) \right\} \tag{2.1}$$

When we choose to work in this context we will refer back to Equation (2.1).

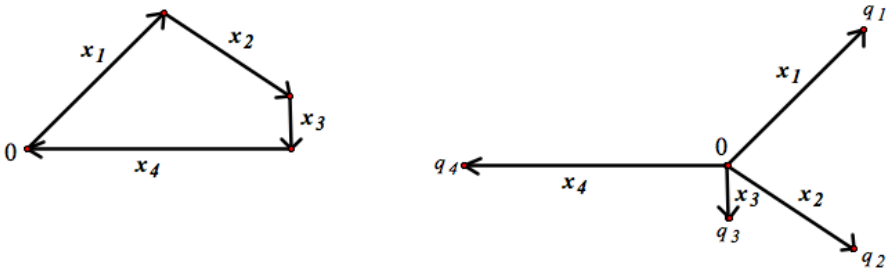

Figure 2.1: For $n = 4$: On the left, the moduli space is viewed as a set of vectors put "head-to-tail", starting at the origin. On the right, the moduli space is viewed as a cloud of points q_i with centroid at the origin.

2.2 Two Ways to View the Moduli Space

There are two ways to view the moduli space $\mathcal{M}(\vec{\ell}, n)$: The first is as a collection of vector sides $\{\mathbf{x}_1, \ldots, \mathbf{x}_n\} \in \mathbb{R}^2$ where the tail of $\mathbf{x}_1$ is at the origin, the tail of $\mathbf{x}_2$ is at the head of $\mathbf{x}_1$, and so on. This is how we see the n-gon shape formed by these vector sides.

The second way is with all vector tails at the origin. We can think of the heads of these vectors as a collection of points with centroid at the origin [7]. In other words, let q_i be the head of vector $\mathbf{x}_i$. Then q_i is a distance ℓ_i away from the centroid, and the centroid of the set $\{q_1, \ldots, q_n\}$ is $(0, 0)$ (See Figure 2.1 for an example where $n = 4$).

It can be useful to switch back and forth between these two viewpoints, and we will do so when convenient. For example, when $\mathcal{M}(\vec{\ell}, n)$ is viewed as a cloud of points with centroid at the origin, it is clearer that the choice of how we label the points is irrelevant for the

topological type of $\mathcal{M}(\vec{\ell}, n)$. In other words, a permutation of the side lengths in $\vec{\ell}$ does not change the topology of the moduli space. This is less clear when viewed as vector sides of n-gons, and we prove this result next.

2.3 Permutations of Side Lengths

As alluded to previously, the order in which the side lengths occur in $\vec{\ell}$ does not change the topology of $\mathcal{M}(\vec{\ell}, n)$.

Theorem 2.3.1. *Let $\sigma : \{1, \ldots, n\} \longrightarrow \{1, \ldots, n\}$ be any permutation. Let $\vec{\ell}_\sigma = (\ell_{\sigma(1)}, \ldots, \ell_{\sigma(n)})$. Then there is a homeomorphism, $\Phi_\sigma : \mathcal{M}(\vec{\ell}, n) \longrightarrow \mathcal{M}(\vec{\ell}_\sigma, n)$.*

Proof. If $\sigma : \{1, \ldots, n\} \longrightarrow \{1, \ldots, n\}$ is any permutation, then σ defines a diffeomorphism

$$\Phi_\sigma : \mathbb{C}^* \times \cdots \times \mathbb{C}^* \longrightarrow \mathbb{C}^* \times \cdots \times \mathbb{C}^*$$

given by

$$\Phi_\sigma(\mathbf{x}_1, \ldots, \mathbf{x}_n) = (\mathbf{x}_{\sigma(1)}, \ldots, \mathbf{x}_{\sigma(n)}).$$

As a permutation of the product's factors, Φ_σ intertwines the $SO(2)$ actions: i.e., for α the action of any element of $SO(2)$, the following diagram commutes:

$$\begin{array}{ccc} \mathcal{PM}(\vec{\ell}, n) & \xrightarrow{\alpha} & \mathcal{PM}(\vec{\ell}, n) \\ \downarrow{\scriptstyle \Phi_\sigma} & & \downarrow{\scriptstyle \Phi_\sigma} \\ \mathcal{PM}(\vec{\ell}_\sigma, n) & \xrightarrow{\alpha} & \mathcal{PM}(\vec{\ell}_\sigma, n) \end{array}$$

Φ_σ is a diffeomorphism of the ambient spaces, hence it is also a homeomorphism. Because $\mathcal{PM}(\vec{\ell}, n)$ inherits the topology (and a smooth structure everywhere but the straight-line configurations) from the ambient space, Φ_σ induces a homeomorphism (diffeomorphism everywhere but the straight-line configurations) from $\mathcal{PM}(\vec{\ell}, n)$ to $\mathcal{PM}(\vec{\ell}_\sigma, n)$. Because Φ_σ commutes with α, the homeomorphism between $\mathcal{PM}(\vec{\ell}, n)$ and $\mathcal{PM}(\vec{\ell}_\sigma, n)$ descends to a homeomorphism of the quotients $\mathcal{M}(\vec{\ell}, n)$ and $\mathcal{M}(\vec{\ell}_\sigma, n)$.

□

Therefore the order in which the side lengths appear in $\vec{\ell}$ is irrelevant for the homeomorphism type of $\mathcal{M}(\vec{\ell}, n)$. This means we can specify an ordering of side lengths that is convenient for proving topological results. Some results are easier to "see" with the side lengths arranged a certain way, even though the result holds no matter what the order. Thus, without loss of generality, we will assume that ℓ_n is the longest side for the remainder of Chapter 2 and all of Chapter 3.

Lemma 2.3.2. *If* $\ell_n > \sum_{i=1}^{n-1} \ell_i$ *then* $\mathcal{M}(\vec{\ell}, n) = \emptyset$.

Proof. For $n = 3$ the lemma holds by the Triangle Inequality. One can use induction to get the result for $n > 3$ [3]. □

Because we are only interested in cases where the moduli space is non-empty, we will always assume that the length of the longest side is less than or equal to the sum of the lengths of all the other sides.

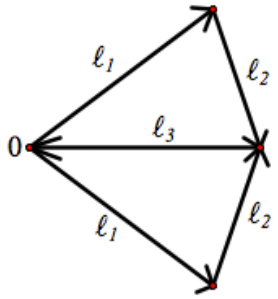

Figure 2.2: Two unique triangles in the moduli space $\mathcal{M}(\vec{\ell}, 3)$.

2.4 The Case $n = 3$

First we will examine the trivial case $n = 3$ to motivate further discussions for $n > 3$. There are two possible cases: either $\ell_3 = \ell_1 + \ell_2$ or $\ell_3 < \ell_1 + \ell_2$. In the former case, the only triangle that can be drawn is degenerate, with all sides collinear with the positive x-axis. In the latter case, two unique (up to affine transformation) triangles can be drawn, which are congruent to each other via a reflection across the x-axis (see Figure 2.2). In the former case the moduli space consists of a single point, while in the latter case the moduli space consists of two distinct points.

In this simple example we see that the moduli space can either be connected or unconnected. We will now use these triangles to motivate the condition for the moduli space to be connected.

2.5 Motivation for Connectedness

Begin with a triangle with sides $A > B \geq C$ such that $A < B + C$. Let side A lie on the x-axis. Let D be small enough that $A < B + C - D$. This creates a "short" fourth side, D (see Figure 2.3). This quadrilateral is (Hausdorff) close to the triangle [5].

If we have

$$\begin{aligned} A &< B + C - D \\ A - B &< C - D \end{aligned}$$

then side B cannot lie along the x-axis because, if it did, we would be able to form a triangle with side lengths $A - B, C$, and D. Then by the triangle inequality we would have $(A - B) + D \geq C$, but this is a contradiction to our assumption. Therefore there is no way to continuously deform quadrilaterals with side B above the x-axis to quadrilaterals with side B below the x-axis. Hence the moduli space with these side lengths must be unconnected.

Continue the process of adding a "short" side to get an n-gon with "three long sides". The authors of [5] use a formalization of this as the condition for $\mathcal{M}(\vec{\ell}, n)$ to be connected. In Section 3.2 we derive specific conditions on $\vec{\ell}$ for $\mathcal{M}(\vec{\ell}, 4)$ to be connected and show that $\mathcal{M}(\vec{\ell}, 4)$ has at most two components.

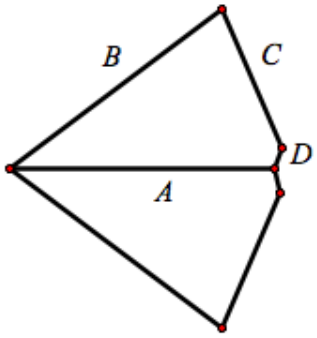

Figure 2.3: Two quadrilaterals with one "short" side.

Chapter 3

Topology of Spaces of Planar Quadrilaterals

For the rest of this paper we will consider the case where $n = 4$, quadrilaterals in the plane. There are lots of results about the topology of these spaces for $n \geq 4$ [2], [5], [6], [8], [10]. We will study the differential geometry of these spaces for $n = 4$. This differential geometry has not been studied for any n. In this chapter we will recall topological results for $n = 4$ with some original proofs as a basis for studying the differential geometry of these spaces.

From now on we will write $\mathcal{M}(\vec{\ell})$ in place of $\mathcal{M}(\vec{\ell}, 4)$ and $\mathcal{PM}(\vec{\ell})$ in place of $\mathcal{PM}(\vec{\ell}, 4)$ for the moduli space and pre-moduli space, respectively.

3.1 Visualizing the Moduli Space

Because the order of the side lengths does not affect the topology of the moduli space (recall Theorem 2.3.1), let $A \geq B \geq C \geq D$ be the side lengths given in non-ascending order. Let $\ell_4 = A$ lie along the x-axis. Let $\ell_1 = B, \ell_2 = C$ and $\ell_3 = D$. Because we are only interested in non-empty moduli spaces, we have assumed that $A \leq B + C + D$ (see Lemma 2.3.2).

Lemma 3.1.1. *If the two shortest sides are adjacent they can always be straightened to form a triangle with side lengths A, B, and C+D.*

Proof. This is clear from the assumption $A \leq B + C + D$. □

So far, $\mathcal{PM}(\vec{\ell})$ and $\mathcal{M}(\vec{\ell})$ have been defined in terms of vector sides. At times it is convenient to define them in terms of vertices, instead. We now give a justification for why we can do this.

Vectors	Vertices
$\mathbf{x}_1$	$p_1 = \mathbf{x}_1 + \mathbf{x}_2 + \mathbf{x}_3 + \mathbf{x}_4$
$\mathbf{x}_2$	$p_2 = \mathbf{x}_1$
$\mathbf{x}_3$	$p_3 = \mathbf{x}_1 + \mathbf{x}_2$
$\mathbf{x}_4$	$p_4 = \mathbf{x}_1 + \mathbf{x}_2 + \mathbf{x}_3$
$\sum_{i=1}^{4} \mathbf{x}_i = \mathbf{0}$	$p_1 = (0, 0)$

There is a diffeomorphism $\Psi : \mathbb{R}^8 \longrightarrow \mathbb{R}^8$ given by

$$\Psi(\mathbf{x}_1, \mathbf{x}_2, \mathbf{x}_3, \mathbf{x}_4) = (\mathbf{x}_1 + \mathbf{x}_2 + \mathbf{x}_3 + \mathbf{x}_4, \mathbf{x}_1, \mathbf{x}_1 + \mathbf{x}_2, \mathbf{x}_1 + \mathbf{x}_2 + \mathbf{x}_3)$$

that identifies the solution sets of the equations $\sum_{i=1}^{4} \mathbf{x}_i = \mathbf{0}$ and $p_1 = (0,0)$ and intertwines the $SO(2)$ actions. Therefore we may also define $\mathcal{M}(\vec{\ell})$ by the coordinates of the vertices, and if we view $\mathcal{M}(\vec{\ell})$ in the context of Equation (2.1) where $\mathbf{x}_4 = (-\ell_4, 0)$ is fixed, the corresponding vertex view fixes $p_4 = (\ell_4, 0)$. Thus a point $m \in \mathcal{M}(\vec{\ell})$ can be represented by $m = (p_2, p_3)$.

3.1.1 The Moduli Space as Intersections of Circles

Notation 3.1.2. Let $\mathcal{C}_1$ be the circle of radius ℓ_1 with center $(0,0)$, $\mathcal{C}_2$ the circle of radius ℓ_2 with center p_2, and $\mathcal{C}_3$ the circle of radius ℓ_3 with center p_4.

Observe that p_2 must lie on the circle $\mathcal{C}_1$, but it cannot be just anywhere on that circle: for example, it can be at most $\ell_2 + \ell_3$ units away from p_4. Thus $p_2 = (a, b)$ lives on some subset of $\mathcal{C}_1$. Similarly, $p_3 = (c, d)$ lives on some subset of $\mathcal{C}_3$.

To formalize this, let $f : \mathcal{M}(\vec{\ell}) \longrightarrow \mathcal{C}_1$ be given by

$$f(a, b, c, d) = (a, b)$$

Clearly f is a continuous map. Let $\mathcal{W} = Im(f) \subseteq \mathcal{C}_1$. Then $\mathcal{W}$ is the subset of circle $\mathcal{C}_1$ on which p_2 may lie.

Now consider the circle $\mathcal{C}_2$, with center p_2. The points where $\mathcal{C}_2$ and $\mathcal{C}_3$ intersect (they must intersect somewhere because we assume the moduli space is non-empty) are the only choices for the placement of p_3, because at all times p_3 must be exactly ℓ_2 units away from p_2 and

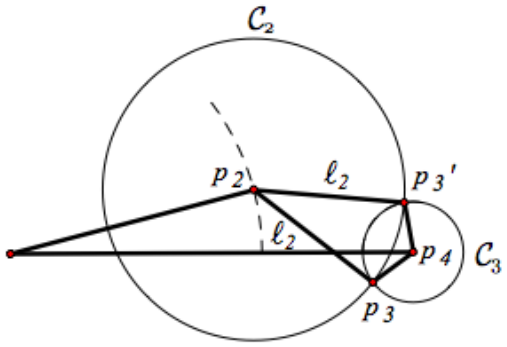

Figure 3.1: For a fixed p_2 there are up to two choices for p_3: the intersection points of $\mathcal{C}_2$ and $\mathcal{C}_3$.

ℓ_3 units away from p_4. Thus for a fixed p_2 there are up to two choices for p_3 resulting from the intersection of $\mathcal{C}_2$ and $\mathcal{C}_3$ (see Figure 3.1). The only exception to this is when $\mathcal{C}_2 = \mathcal{C}_3$, but this only happens for very special choices of side lengths.

If p_2 is at an endpoint of $\mathcal{W}$ that lies farthest away from p_4, this corresponds to $\mathcal{C}_2$ and $\mathcal{C}_3$ touching at a single point. This corresponds to ℓ_2 and ℓ_3 being straightened to form a triangle and hence only one choice for p_3. We give this quadrilateral a special name and definition.

Definition 3.1.3. Define the $\triangle$-*configuration* to be the quadrilateral where ℓ_2 is straightened with an adjacent side (in this case ℓ_3).

Observe that there are always two $\triangle$-configurations in $\mathcal{M}(\vec{\ell})$ related by a reflection across the x-axis. In fact, for any point $m \in \mathcal{M}(\vec{\ell})$ there is a corresponding point $m' \in \mathcal{M}(\vec{\ell})$ which is a reflection of all the vector sides across the x-axis.

3.2 Connectedness

We now show that $\mathcal{M}(\vec{\ell})$ has at most two connected components and we give a condition on side lengths to guarantee the connectedness of $\mathcal{M}(\vec{\ell})$. Recall that $f : \mathcal{M}(\vec{\ell}) \longrightarrow \mathcal{C}_1$ is given by $f(a, b, c, d) = (a, b)$, and $\mathcal{W} = Im(f)$.

Definition 3.2.1. Define $\mathcal{W}^+ = \{(a, b) \in \mathcal{W} : b \geq 0\} \subseteq \mathcal{W}$.

Definition 3.2.2. Define $\mathcal{W}^- = \{(a, b) \in \mathcal{W} : b \leq 0\} \subseteq \mathcal{W}$.

Lemma 3.2.3. *The sets $\mathcal{W}^+$ and $\mathcal{W}^-$ are connected.*

Proof. We will show that $\mathcal{W}^+$ is connected. The proof for $\mathcal{W}^-$ connected is analogous.

Let $(a(u), b(u)) = (\ell_1 \cos(u), \ell_1 \sin(u))$ be the parametrization of points on the circle $\mathcal{C}_1$ with $b(u) \geq 0$. Let u_0 be the angle corresponding to the $\triangle$-configuration with $b_0 = b(u_0) \geq 0$ and observe that u_0 is a maximum value for u. At the point $(a(u_0), b(u_0))$, the distance from $(\ell_4, 0)$ to $(a(u_0), b(u_0)) = (a_0, b_0)$ is equal to $\ell_2 + \ell_3$.

Let $\delta(u) = \sqrt{(a(u) - \ell_4)^2 + b(u)^2}$ be the distance from p_2 to p_4 at angle u. Then $\delta(u_0) = \ell_2 + \ell_3$. Observe that the possible range of values for $\delta(u)$ is: $\ell_2 - \ell_3 \leq \delta(u) \leq \ell_2 + \ell_3$. Also observe that, if u is such that $\delta(u)$ falls in this range, then the circles $\mathcal{C}_2$ and $\mathcal{C}_3$ intersect and hence for angle u there is at least one corresponding point in the moduli space. The function $\delta(u)$ is monotonic in u.

Now let u_1 be such that $(a(u_1), b(u_1)) \in \mathcal{W}^+$. Observe that $u_1 = u_0 - C$, where $0 \leq C \leq u_0$. Define $\gamma : [0, 1] \longrightarrow [u_1, u_0]$ by $\gamma(t) = u_0 - tC$. Then $\gamma(0) = u_0$ and $\gamma(1) = u_1$. Let

$(a(t), b(t)) = (\ell_1 \cos(\gamma(t)), \ell_1 \sin(\gamma(t)))$ be a parametrization. Observe that this path remains in $\mathcal{W}^+$ for two reasons: the first is because $0 \leq u_1 \leq u_0 \leq \pi$ and so $b(t) \geq 0$ on $[0, 1]$, the second is because for any u such that $u_1 \leq u \leq u_0$, the function $\delta(u)$ falls into the range of values required to have circles $\mathcal{C}_2$ and $\mathcal{C}_3$ intersect; hence the point $(a(u), b(u))$ is in the image of f.

□

Lemma 3.2.4. *The sets $f^{-1}(\mathcal{W}^+)$ and $f^{-1}(\mathcal{W}^-)$ are connected.*

Proof. We will show that $f^{-1}(\mathcal{W}^+)$ is path connected, hence connected. The proof for $f^{-1}(\mathcal{W}^-)$ is analogous. Recall we have assumed that $\ell_4 \geq \ell_1 \geq \ell_2 \geq \ell_3$.

By Lemma 3.1.1 we can straighten ℓ_2 and ℓ_3 to form a triangle. Let $m_0 = (a_0, b_0, c_0, d_0) \in f^{-1}(\mathcal{W}^+)$ be the $\triangle$-configuration and let $m_1 = (a_1, b_1, c_1, d_1) \in f^{-1}(\mathcal{W}^+)$ be any other point. We will exhibit a path from m_0 to m_1 that remains in $f^{-1}(\mathcal{W}^+)$.

Because $f(m_0) = (a_0, b_0) \in \mathcal{W}^+, f(m_1) = (a_1, b_1) \in \mathcal{W}^+$, and $\mathcal{W}^+$ is path connected (by Lemma 3.2.3), there exists a continuous map $\gamma : [0, 1] \longrightarrow \mathcal{W}^+$ such that $\gamma(0) = (a_0, b_0)$ and $\gamma(1) = (a_1, b_1)$ given by $\gamma(t) = (a(t), b(t))$.

We now use the Implicit Mapping Theorem on the two equations:

$$\begin{aligned} (c-a)^2 + (d-b)^2 &= \ell_2^2 \\ (\ell_4 - c)^2 + d^2 &= \ell_3^2 \end{aligned}$$

to show that (c, d) can be written as a function of (a, b). The Jacobian matrix is:

$$\begin{bmatrix} -2(c-a) & -2(d-b) & 2(c-a) & 2(d-b) \\ 0 & 0 & -2(\ell_4 - c) & 2d \end{bmatrix}$$

In order to guarantee that (c, d) can be written as a function of (a, b), we need the rows of the matrix

$$\begin{bmatrix} 2(c-a) & 2(d-b) \\ -2(\ell_4 - c) & 2d \end{bmatrix}$$

to be linearly independent. Observe that this happens everywhere but at the points where $(c - a, d - b)$ and $(\ell_4 - c, -d)$ are parallel. Note that one place this happens is at the $\triangle$-configuration. We now explicitly define a continuous extension to the $\triangle$-configuration.

Recall that (a_0, b_0, c_0, d_0) are the coordinates of the $\triangle$-configuration. Let $(a(u), b(u)) = (\ell_1 \cos(u), \ell_1 \sin(u))$ and $(a(u_0), b(u_0)) = (a_0, b_0)$. Then $(a(u), b(u))$ is a continuous function of u through u_0 and, by the Implicit Mapping Theorem, $(c(u), d(u))$ is a continuous function of u up to u_0. Define $(c(u_0), d(u_0)) = (c_0, d_0)$. We will now prove that this is a continuous extension of $(c(u), d(u))$ through u_0.

Let $\epsilon = |(a, b) - (a_0, b_0)|$. Then $\epsilon \to 0$ as $u \to u_0$. Let $\delta = |(c, d) - (c_0, d_0)|$. We will show that $\delta \to 0$ as $\epsilon \to 0$.

Consider the triangle formed by the points $(a_0, b_0), (c_0, d_0)$ and (c, d). This triangle has side lengths $\ell_2, \ell_2 + \epsilon$, and δ (see Figure 3.2). The dotted line ℓ shown in Figure 3.2 passes through (c_0, d_0) and is tangent to both circles $\mathcal{C}_2$ and $\mathcal{C}_3$. Therefore the line ℓ is orthogonal to both radii and hence the two circles $\mathcal{C}_2$ and $\mathcal{C}_3$ lie on opposite sides of the tangent line ℓ. Let Φ

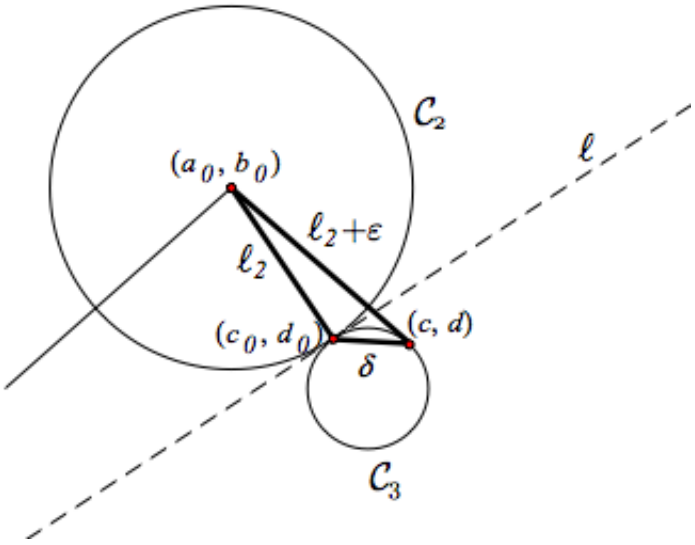

Figure 3.2: The triangle formed by the points $(a_0, b_0), (c_0, d_0)$ and (c, d) (in bold) has side lengths $\ell_2, \ell_2 + \epsilon$, and δ.

be the angle at (c_0, d_0) (not labeled in the figure). Then because (c, d) is a point on circle $\mathcal{C}_3$, the angle Φ is always obtuse.

By the Law of Cosines, $(\ell_2 + \epsilon)^2 = \ell_2^2 + \delta^2 - 2\ell_2\delta\cos(\Phi)$. Because Φ is obtuse, $\cos(\Phi) \leq 0$. Therefore the term $-2\ell_2\delta\cos(\Phi) \geq 0$. This implies that $\ell_2^2 + \delta^2 \leq (\ell_2 + \epsilon)^2$ and hence $\delta^2 \leq (\ell_2 + \epsilon)^2 - \ell_2^2$. It is now clear that $\delta \to 0$ as $\epsilon \to 0$. Therefore $(c(u), d(u))$ has a continuous extension through u_0.

The other point where $(c - a, d - b)$ and $(\ell_4 - c, -d)$ are parallel occurs only when $\mathcal{W}$ is unconnected. This point corresponds to $\mathbf{x}_2$ and $\mathbf{x}_3$ pointing in opposite directions. We call this point m_2. We now explicitly define a continuous extension of $(c(a, b), d(a, b))$ to the point m_2.

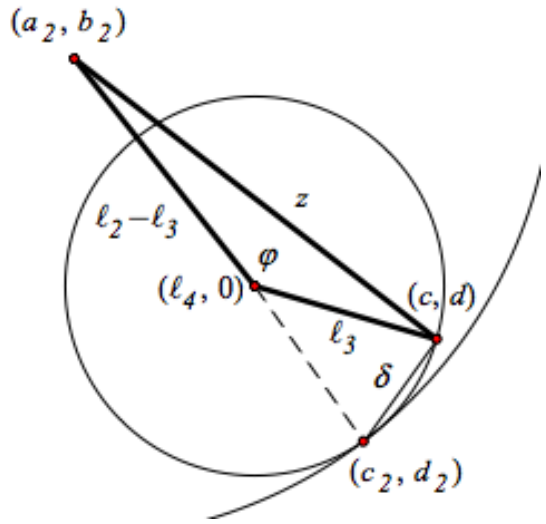

Figure 3.3: The triangle formed by the points $(a_2, b_2), (\ell_4, 0)$ and (c, d) (in bold) has side lengths $\ell_2 - \ell_3, \ell_3$, and z.

Let $m_2 = (a_2, b_2, c_2, d_2)$ be the coordinates. Let u_2 be the angle such that $(a(u_2), b(u_2)) = (a_2, b_2)$. Then $(a(u), b(u))$ is a continuous function of u through u_2 and, by the Implicit Mapping Theorem, $(c(u), d(u))$ is a continuous function of u up to u_2. Define $(c(u_2), d(u_2)) = (c_2, d_2)$. We will now prove that this is a continuous extension of $(c(u), d(u))$.

Let $\epsilon = |(a, b) - (a_2, b_2)|$. Then $\epsilon \to 0$ as $u \to u_2$. Let $\delta = |(c, d) - (c_2, d_2)|$. We will show that $\delta \to 0$ as $\epsilon \to 0$.

Consider the triangle formed by the points $(a_2, b_2), (\ell_4, 0)$, and (c, d). Let $z = |(c, d) - (a_2, b_2)|$. Then this triangle has side lengths $\ell_2 - \ell_3, \ell_3$, and z (see Figure 3.3). Observe that $\ell_2 - \epsilon \leq z \leq \ell_2 + \epsilon$. Let ϕ be the angle at $(\ell_4, 0)$ as shown in Figure 3.3. We will show that $\phi \to \pi$ as $\epsilon \to 0$. By Figure 3.3 it is clear that if $\phi \to \pi$ then $\delta \to 0$.

By the Law of Cosines,

$$\begin{aligned}(\ell_2 \pm \epsilon)^2 &= \ell_3^2 + (\ell_2 - \ell_3)^2 - 2\ell_3(\ell_2 - \ell_3)\cos\phi \\ &= \ell_3^2 + \ell_2^2 + \ell_3^2 - 2\ell_2\ell_3 - 2\ell_2\ell_3\cos\phi + 2\ell_3^2\cos\phi\end{aligned}$$

This implies that

$$(\ell_2 \pm \epsilon)^2 - \ell_2^2 = 2\ell_3(\ell_3 - \ell_2)(1 + \cos\phi) \tag{3.1}$$

Because the left-hand side of Equation (3.1) goes to zero as $\epsilon \to 0$, the right-hand side of Equation (3.1) must also go to zero as $\epsilon \to 0$. But the only term on the right-hand side of Equation (3.1) that can ever equal zero is $1 + \cos\phi$. Therefore $1 + \cos\phi \to 0$ as $\epsilon \to 0$ and hence $\phi \to \pi$ as $\epsilon \to 0$. We have now shown that $\delta \to 0$ as $\epsilon \to 0$ and thus $(c(u), d(u))$ has a continuous extension through u_2.

Thus we can always write $(c(a,b), d(a,b))$, and (a,b) can be written as a function of t. We now have a path $\mathbf{m} : [0,1] \longrightarrow f^{-1}(\mathcal{W}^+)$ given by $\mathbf{m}(t) = (a(t), b(t), c(t), d(t))$ where $\mathbf{m}(0) = m_0$ and $\mathbf{m}(1) = m_1$.

We have shown that for any point in $f^{-1}(\mathcal{W}^+)$ there is a path from $m_0 \in f^{-1}(\mathcal{W}^+)$ to that point which remains in $f^{-1}(\mathcal{W}^+)$. Therefore $f^{-1}(\mathcal{W}^+)$ is path connected, hence connected.

□

It is clear that $\mathcal{W} = \mathcal{W}^+ \cup \mathcal{W}^-$. Therefore $\mathcal{W}$ is connected if and only if $\mathcal{W}^+ \cap \mathcal{W}^- \neq \emptyset$. It is also clear that $\mathcal{M}(\vec{\ell}) = f^{-1}(\mathcal{W}^+) \cup f^{-1}(\mathcal{W}^-)$. Therefore $\mathcal{M}(\vec{\ell})$ is connected if and only if $f^{-1}(\mathcal{W}^+) \cap f^{-1}(\mathcal{W}^-) \neq \emptyset$.

Lemma 3.2.5. *$\mathcal{W}^+ \cap \mathcal{W}^- \neq \emptyset$ if and only if $f^{-1}(\mathcal{W}^+) \cap f^{-1}(\mathcal{W}^-) \neq \emptyset$.*

Proof. Suppose $\mathcal{W}^+ \cap \mathcal{W}^- \neq \emptyset$ so there exists $(a, 0) \in \mathcal{W}^+ \cap \mathcal{W}^-$. By the definitions of the sets involved, any point in $f^{-1}(a, 0)$ is in $f^{-1}(\mathcal{W}^+) \cap f^{-1}(\mathcal{W}^-)$ and hence $f^{-1}(\mathcal{W}^+) \cap f^{-1}(\mathcal{W}^-) \neq \emptyset$. Now suppose $f^{-1}(\mathcal{W}^+) \cap f^{-1}(\mathcal{W}^-) \neq \emptyset$. Then there exists $m \in f^{-1}(\mathcal{W}^+) \cap f^{-1}(\mathcal{W}^-)$ and $f(m) \in \mathcal{W}^+ \cap \mathcal{W}^-$. Therefore $\mathcal{W}^+ \cap \mathcal{W}^- \neq \emptyset$.

□

Therefore, to show that $\mathcal{M}(\vec{\ell})$ is connected, it suffices to show that $\mathcal{W}^+ \cap \mathcal{W}^- \neq \emptyset$. There are only two points that could be in the intersection of $\mathcal{W}^+$ and $\mathcal{W}^-$: the point $(-\ell_1, 0)$ and the point $(\ell_1, 0)$.

Claim 3.2.6. *Since $\ell_4 \geq \ell_1 \geq \ell_2 \geq \ell_3$, then $(-\ell_1, 0) \in \mathcal{W}$ if and only if $\ell_1 = \ell_2 = \ell_3 = \ell_4$.*

Proof. If $(-\ell_1, 0) \in \mathcal{W}$, observe that $\ell_1 + \ell_4 = \ell_2 + \ell_3$. This happens if and only if all the side lengths are equal.

□

Note that in the case of equal side lengths, $(\ell_1, 0) \in \mathcal{W}$. Now assume that all the side lengths are not equal. Then $\mathcal{W}$ (and hence $\mathcal{M}(\vec{\ell})$) is connected if and only if $(\ell_1, 0) \in \mathcal{W}$.

3.2.1 Condition on Side Lengths for Connectedness

Theorem 3.2.7. *Let $A \geq B \geq C \geq D$ be the four given side lengths arranged in non-ascending order. Then $\mathcal{M}(\vec{\ell})$ is connected if and only if $C - D \leq A - B$.*

Proof. Again let $\vec{\ell} = (B, C, D, A)$ and assume that we are not in the case $A = B = C = D$, so that $(-B, 0) \notin \mathcal{W}$. Then by our previous discussion, $\mathcal{M}(\vec{\ell})$ is connected if and only if $(B, 0) \in \mathcal{W}$.

Assume first that $A > B$. Then $(B, 0) \in \mathcal{W}$ if and only if the side lengths $A - B, C$, and D can form a triangle. By the triangle inequality, this is true if and only if $C \leq (A - B) + D$, ie, if and only if $C - D \leq A - B$.

If $A = B$, then $(B, 0) \in \mathcal{W}$ if and only if $C = D$, in which case $C - D \leq A - B$ is trivially satisfied.

If we are in the case $A = B = C = D$ then $C - D \leq A - B$ is trivially satisfied. □

3.3 Classification

Here we state the results of previous authors about the topology of the moduli space of planar quadrilaterals. We will use examples in the next section to illustrate each specific case.

Theorem 3.3.1. *Let $\vec{\ell} = (\ell_1, \ell_2, \ell_3, \ell_4)$ be given such that $\ell_4 \leq \sum_{i=1}^{3} \ell_i$ (this is just a restate-*

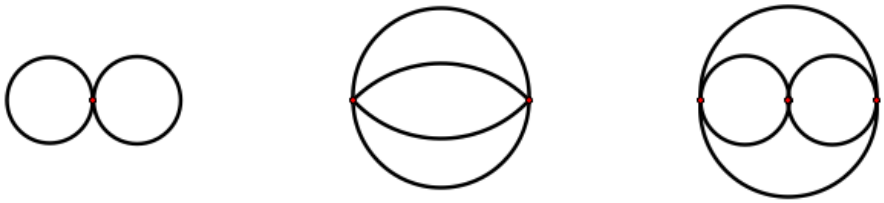

Figure 3.4: The moduli space for case *(d)* on the left, *(e)* in the center, and *(f)* on the right.

ment of our previous assumptions preventing the moduli space from being the empty set). Then the moduli space $\mathcal{M}(\vec{\ell})$ is homeomorphic to one of the following:

(a) A point

(b) A circle, $\mathcal{S}^1$

(c) Two disjoint circles, $\mathcal{S}^1 \sqcup \mathcal{S}^1$

(d) Two circles touching at a single point, $\mathcal{S}^1 \vee \mathcal{S}^1$

(e) Two circles touching at two distinct points, $\mathcal{S}^1 \vee_2 \mathcal{S}^1$

(f) Three circles, each touching the other circle at one distinct point, $(\mathcal{S}^1 \vee \mathcal{S}^1) \vee_2 \mathcal{S}^1$

Proof. For a formal proof see [5]. These results are well-known. See Figure 3.4 for illustrations of *(d), (e)* and *(f).* □

Recall that $\mathcal{M}(\vec{\ell})$ is a 1-manifold everywhere but at the straight-line configurations. The straight-line configurations appear as the points where circles in the moduli space intersect, as seen in cases (d) (one straight-line configuration), (e) (two straight-line configurations) and (f) (three straight-line configurations).

We will now give examples of cases (b) through (f) with proofs of (e) and (f).

3.4 Examples

3.4.1 Case (b)

Example 3.4.1. Let $\vec{\ell} = (5, 3, 1, 8)$. For these side lengths the moduli space is homeomorphic to $\mathcal{S}^1$.

To see this, fix ℓ_4 along the positive x-axis and straighten $\mathbf{x}_2$ and $\mathbf{x}_3$. Then the resulting shape is a triangle with side lengths 5, 4, and 8. We can think of p_2 moving down towards the x-axis, pushing the other two sides out. As p_2 continues its descent towards the x-axis, $\mathbf{x}_2$ and $\mathbf{x}_3$ are pulled down. The point p_2 can pass through the x-axis, continuing to pull the other two sides with it, until it reaches its lowest point. Here $\mathbf{x}_2$ and $\mathbf{x}_3$ are straightened again, forming the original triangle reflected across the x-axis. Then as p_2 moves back up it pulls $\mathbf{x}_2$ and $\mathbf{x}_3$ back with it, mirroring the trip down and returning to the top triangle (see Figure 3.5). Because this trip passes through all possible quadrilaterals with these side lengths, the moduli space is homeomorphic to a circle.

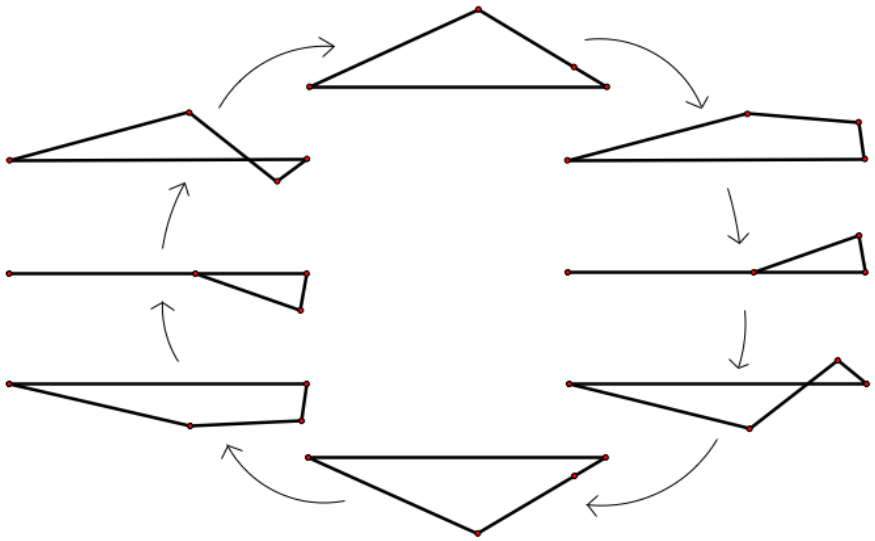

Figure 3.5: The circle of quadrilaterals with sides lengths $\vec{\ell} = (5, 3, 1, 8)$.

3.4.2 Case (c)

Example 3.4.2. Let $\vec{\ell} = (5, 3, 1, 6)$. For these side lengths the moduli space is homeomorphic to $\mathcal{S}^1 \sqcup \mathcal{S}^1$.

Here p_2 cannot lie on the x-axis because $3 - 1 > 6 - 5$. Thus in this example the moduli space is homeomorphic to two circles, one corresponding to p_2 lying above the x-axis and the other corresponding to p_2 lying below the x-axis. Because p_2 cannot pass through the x-axis, the moduli space is unconnected. The quadrilaterals in the lower circle correspond to the quadrilaterals in the upper circle by a reflection across the x-axis. See Figure 3.6 for an illustration of the quadrilaterals in the upper circle.

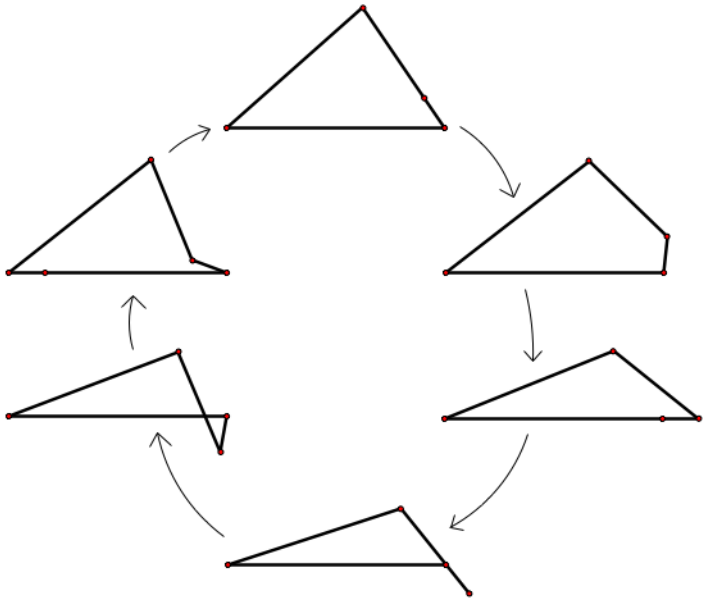

Figure 3.6: The circle of quadrilaterals with p_2 above the x-axis for $\vec{\ell} = (5, 3, 1, 6)$.

3.4.3 Case (d)

Example 3.4.3. Let $\vec{\ell} = (5, 3, 1, 7)$. For these side lengths the moduli space is homeomorphic to $\mathcal{S}^1 \vee \mathcal{S}^1$.

Because $7 = 5 + 3 - 1$, a degenerate quadrilateral can be formed in the following way: $\mathbf{x}_1$ points to the right, $\mathbf{x}_2$ points to the right, $\mathbf{x}_3$ points to the left and $\mathbf{x}_4$ points to the left. All the sides are collinear, and this quadrilateral corresponds to the intersection point of the two circles in the moduli space.

One circle represents the quadrilaterals with p_2 above the x-axis and the other circle represents the quadrilaterals with p_2 below the x-axis. Because p_2 can pass through the x-axis

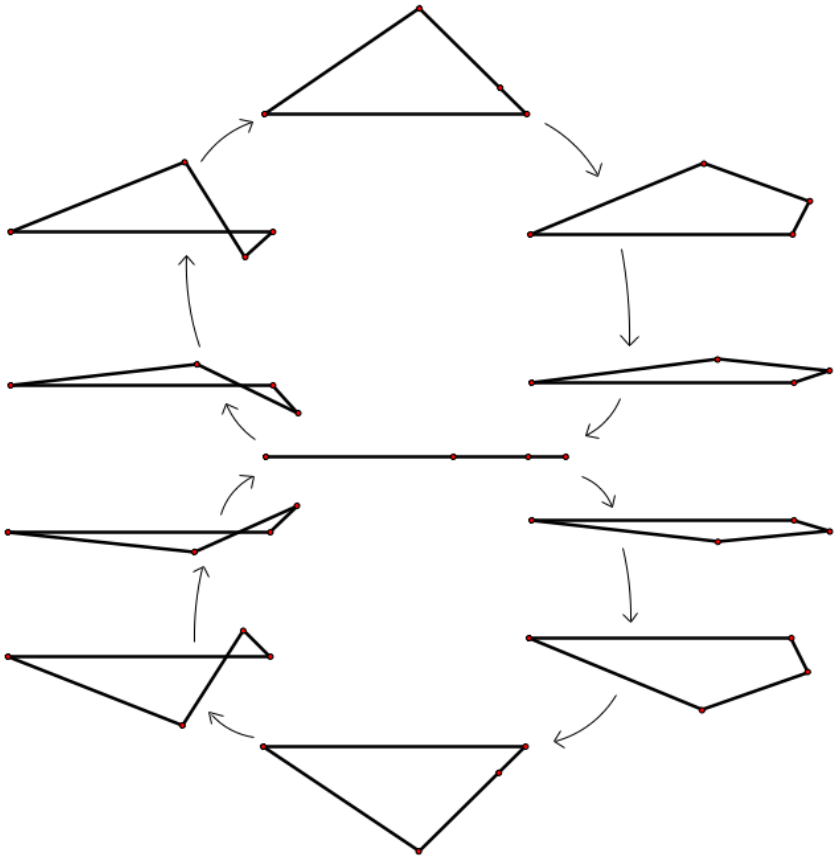

Figure 3.7: The moduli space of quadrilaterals with side lengths $\vec{\ell} = (5, 3, 1, 7)$.

via the degenerate quadrilateral, the moduli space is connected. See Figure 3.7.

3.4.4 Case (e)

We will refer to this case as the *rectangle* case, meaning that two sides are of equal length and the other two sides of a different equal length. The moduli space is homeomorphic to $\mathcal{S}^1 \vee_2 \mathcal{S}^1$ (see Figure 3.8).

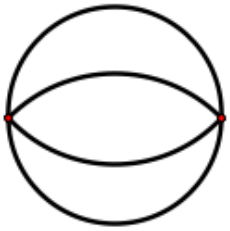

Figure 3.8: The moduli space for Case (e), the rectangle case.

Example 3.4.4. Let $\vec{\ell} = (1, 5, 1, 5)$.

Here there are two distinct degenerate quadrilaterals: the first with $\mathbf{x}_1$ pointing to the right, $\mathbf{x}_2$ pointing to the right, $\mathbf{x}_3$ pointing to the left, and $\mathbf{x}_4$ pointing to the left; the second with $\mathbf{x}_1$ pointing to the left, $\mathbf{x}_2$ pointing to the right, $\mathbf{x}_3$ pointing to the right, and $\mathbf{x}_4$ pointing to the left. The two degenerate quadrilaterals are represented in the moduli space by the intersection points of the two circles.

We now give a proof that the moduli space for the rectangle case must be homeomorphic to $\mathcal{S}^1 \vee_2 \mathcal{S}^1$ based on a path analysis.

Theorem 3.4.5. *Let $l, s > 0$ be given such that $l > s$ and let $\vec{\ell} = (l, l, s, s)$ be the given side lengths for a quadrilateral, in no particular order. Then $\mathcal{M}(\vec{\ell})$ is homeomorphic to $\mathcal{S}^1 \vee_2 \mathcal{S}^1$.*

Proof. Since we have already proved that the order in which the side lengths appear in $\vec{\ell}$ does not change the topology of $\mathcal{M}(\vec{\ell})$ (see Theorem 2.3.1), we will choose an order that is convenient. Let $\vec{\ell} = (s, l, s, l)$.

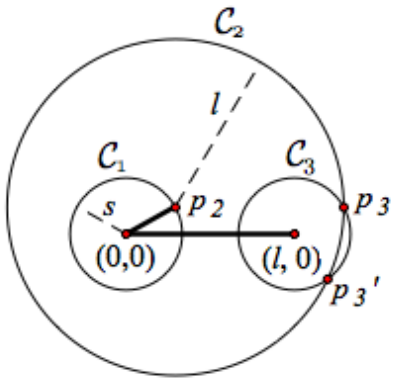

Figure 3.9: For a fixed p_2, the possible choices for p_3 are the intersection points of circles $\mathcal{C}_2$ and $\mathcal{C}_3$.

Recall that we are working in the context of Equation (2.1), where $p_1 = (0, 0)$ and $p_4 = (l, 0)$ are fixed, p_2 lies on circle $\mathcal{C}_1$ which has center $(0, 0)$ and radius s, and p_3 lies on circle $\mathcal{C}_3$ which has center $(l, 0)$ and radius s. Circle $\mathcal{C}_2$ has center p_2 and radius l. For a fixed p_2, the choices for p_3 are the intersection points of $\mathcal{C}_2$ and $\mathcal{C}_3$ (see Figure 3.9).

Note that, because of the order of the side lengths, p_2 may lie anywhere on circle $\mathcal{C}_1$. Because p_2 is the center of $\mathcal{C}_2$, and we are interested in the intersection points of $\mathcal{C}_2$ and $\mathcal{C}_3$, we examine how "close" p_2 is to p_4.

The closest p_2 can be to p_4 is when p_2 lies on the x-axis at coordinates $p_2 = (s, 0)$. In this case, $\mathcal{C}_2$ and $\mathcal{C}_3$ intersect at a single point, yielding one choice for p_3. That choice corresponds to p_3 also on the x- axis at coordinates $p_3 = (l + s, 0)$. This is one of the straight-line configurations, where the first side points to the right, the second side points to the right, the third side points to the left and the fourth side points to the left. We will

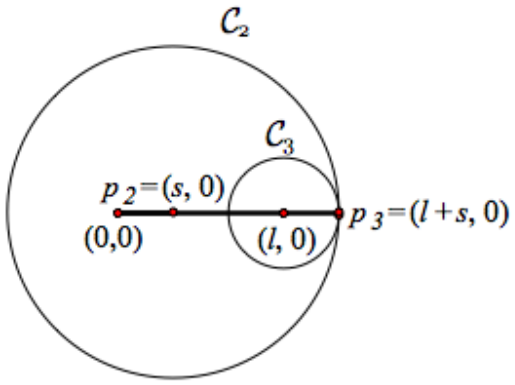

Figure 3.10: Straight-line configuration $\mathcal{A}$.

call this straight-line configuration $\mathcal{A}$ (see Figure 3.10).

The farthest p_2 can be from p_4 is when p_2 is at coordinates $p_2 = (-s, 0)$. In this case, $\mathcal{C}_2$ and $\mathcal{C}_3$ again intersect at a single point, yielding one choice for p_3 at coordinates $p_3 = (l - s, 0)$. This is the other straight-line configuration, with the first side pointing to the left, the second side pointing to the right, the third side pointing to the right and the fourth side pointing to the left. We will call this straight-line configuration $\mathcal{B}$ (see Figure 3.11).

Note that $\mathcal{A}$ and $\mathcal{B}$ are distinct configurations. We now show that there are four distinct paths from $\mathcal{A}$ to $\mathcal{B}$ (or vice versa).

Starting at $\mathcal{A}$, the point p_2 has two options in moving to $\mathcal{B}$: it can either trace out the upper half $\mathcal{C}_1$ that lies above the x-axis, or it can trace out the lower half of $\mathcal{C}_1$ that lies below the x-axis. We will examine the case where p_2 stays above the x-axis. The other case is analogous.

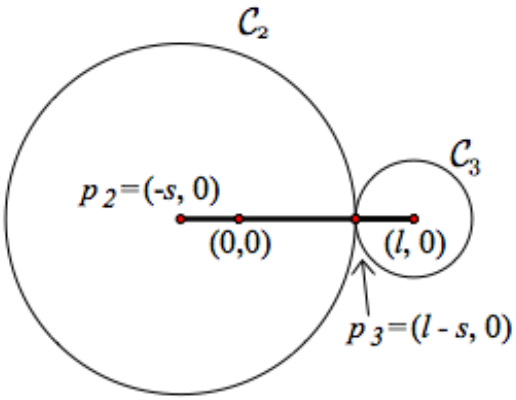

Figure 3.11: Straight-line configuration $\mathcal{B}$.

As p_2 leaves its location at $\mathcal{A}$, moving along $\mathcal{C}_1$ towards $\mathcal{B}$, the circles $\mathcal{C}_2$ and $\mathcal{C}_3$ intersect in two places: one choice for p_3 lies above the x-axis and the other choice lies below the x-axis (see Figure 3.12). We can think of these two choices for p_3 as tracing out the circle $\mathcal{C}_3$ in their journey to $\mathcal{B}$. It is clear that one choice will always be below the x-axis and the other choice will always be above the x-axis. The two choices meet up on the x- axis when they get to $\mathcal{B}$.

We have exhibited two distinct paths from $\mathcal{A}$ to $\mathcal{B}$: 1. The point p_2 remains above the x-axis and p_3 also remains above the x-axis on the entire journey, or 2. the point p_2 remains above the x-axis and p_3 remains below the x-axis on the entire journey. We can make the same argument with p_2 remaining below the x-axis as it moves from $\mathcal{A}$ to $\mathcal{B}$ to get two more distinct paths. Thus there are a total of four distinct paths from $\mathcal{A}$ to $\mathcal{B}$. □

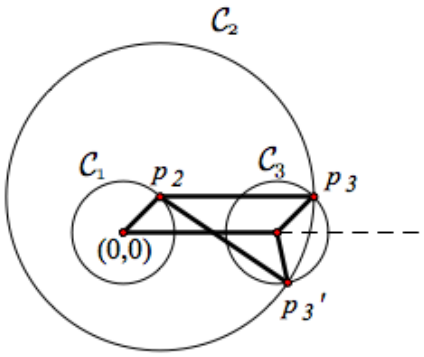

Figure 3.12: Two choices for p_3: one always lies above the x-axis and the other always lies below the x-axis.

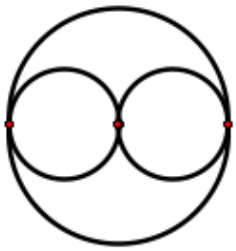

Figure 3.13: The moduli space for the square case.

3.4.5 Case (f)

We will refer to this case as the *square* case, where all four sides are of equal length. Here the moduli space is homeomorphic to $(\mathcal{S}^1 \vee \mathcal{S}^1) \vee_2 \mathcal{S}^1$ (see Figure 3.13)

Example 3.4.6. Let $\vec{\ell} = (2, 2, 2, 2)$.

Here there are three distinct degenerate quadrilaterals:

1. $\mathbf{x}_1$ points to the right, $\mathbf{x}_2$ points to the right, $\mathbf{x}_3$ points to the left, and $\mathbf{x}_4$ points to the left.

2. $\mathbf{x}_1$ points to the left, $\mathbf{x}_2$ points to the right, $\mathbf{x}_3$ points to the right, and $\mathbf{x}_4$ points to the left.

3. $\mathbf{x}_1$ points to the right, $\mathbf{x}_2$ points to the left, $\mathbf{x}_3$ points to the right, and $\mathbf{x}_4$ points to the left.

The three degenerate quadrilaterals are represented in the moduli space by the intersection points of the three circles.

We now give a proof that the moduli space for the square must be homeomorphic to $(\mathcal{S}^1 \vee \mathcal{S}^1) \vee_2 \mathcal{S}^1$ based on a path analysis.

Theorem 3.4.7. *Let $s > 0$ and $\vec{\ell} = (s, s, s, s)$ be the given side lengths for a quadrilateral. Then $\mathcal{M}(\vec{\ell})$ is homeomorphic to $(\mathcal{S}^1 \vee \mathcal{S}^1) \vee_2 \mathcal{S}^1$.*

Proof. First note that $\mathcal{C}_1$ has center $(0, 0)$ and radius s, $\mathcal{C}_2$ has center p_2 and radius s, and $\mathcal{C}_3$ has center $(s, 0)$ and radius s (see Figure 3.14).

Observe that $\mathcal{C}_2$ always passes through $(0, 0)$, no matter where p_2 lies on circle $\mathcal{C}_1$. Also note that the side lengths allow p_2 to lie anywhere on $\mathcal{C}_1$, i.e., $\mathcal{W} = \mathcal{C}_1$. Circle $\mathcal{C}_3$ also always passes through $(0, 0)$, so $(0, 0)$ is *always* a point of intersection of $\mathcal{C}_2$ and $\mathcal{C}_3$. Hence, $(0, 0)$ is always a choice for p_3.

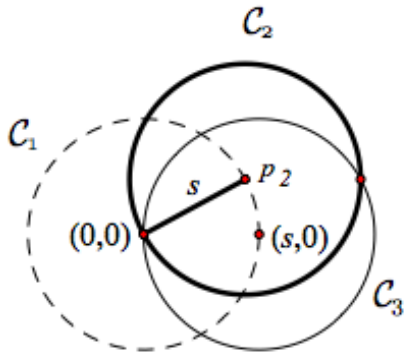

Figure 3.14: $\mathcal{C}_1$ is the dotted circle, $\mathcal{C}_2$ is the bold circle, and $\mathcal{C}_3$ is the thin circle. Note that only $\mathcal{C}_2$ moves.

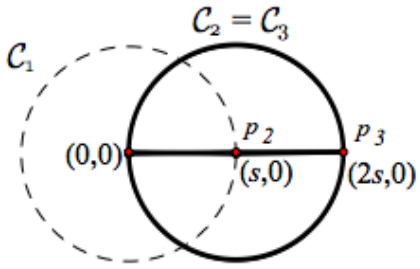

Figure 3.15: Straight-line configuration $\mathcal{A}$.

Once again we are interested in the intersection points of $\mathcal{C}_2$ and $\mathcal{C}_3$. When $p_2 = (s, 0)$, the circles $\mathcal{C}_2$ and $\mathcal{C}_3$ sit on top of one another, so there are infinitely many choices for p_3 without changing p_2. When $p_3 = (2s, 0)$ all the sides are collinear. We call this straight-line configuration $\mathcal{A}$ (see Figure 3.15).

When $p_3 = (0, 0)$, all the sides are collinear as well. We call this straight-line configuration $\mathcal{B}$ (see Figure 3.16).

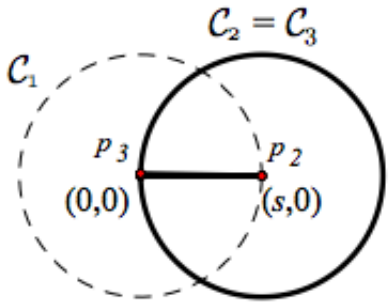

Figure 3.16: Straight-line configuration $\mathcal{B}$.

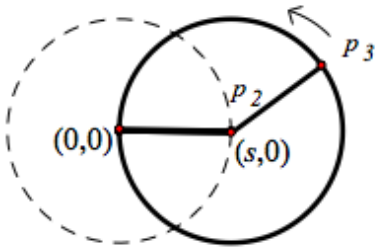

Figure 3.17: Moving from $\mathcal{A}$ to $\mathcal{B}$ with p_3 above the x-axis and p_2 fixed at $(s, 0)$.

In moving from $\mathcal{A}$ to $\mathcal{B}$, the point p_3 can either move above the x-axis along $\mathcal{C}_3$ or it can move below the x-axis along $\mathcal{C}_3$. Either choice defines a different path from $\mathcal{A}$ to $\mathcal{B}$. Note that p_2 does not move at all on either of these paths! Thus there are two distinct paths between $\mathcal{A}$ and $\mathcal{B}$, both keeping p_2 fixed at $(s, 0)$ (see Figure 3.17).

Now fix $p_2 = (-s, 0)$. Then $\mathcal{C}_2$ and $\mathcal{C}_3$ intersect only at one point, $(0, 0)$. This choice for p_3 gives the third straight-line configuration $\mathcal{C}$ (see Figure 3.18). Note that $\mathcal{A}, \mathcal{B}$, and $\mathcal{C}$ are all distinct.

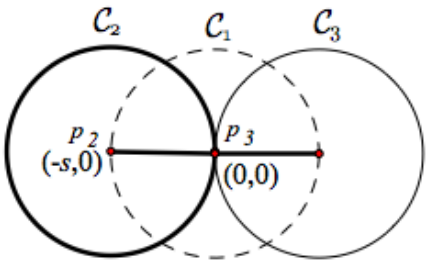

Figure 3.18: Straight-line configuration $\mathcal{C}$.

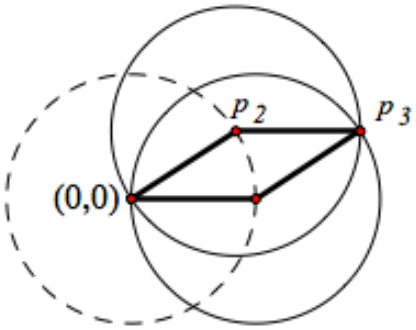

Figure 3.19: Moving from $\mathcal{A}$ to $\mathcal{C}$ with p_2 (and hence p_3) above the x-axis.

In moving from $\mathcal{A}$ to $\mathcal{C}$, the point p_2 can move either above or below the x-axis along $\mathcal{C}_1$. At any choice for p_2 above the x-axis, $\mathcal{C}_2$ and $\mathcal{C}_3$ intersect in two places. One of the intersection points is always $(0, 0)$.

Starting at $\mathcal{A}$, the point p_3 starts at $(2s, 0)$. As p_2 moves along $\mathcal{C}_1$, the point p_3 can't "jump" from $(2s, 0)$ to $(0, 0)$ continuously. So, leaving $\mathcal{A}$, there is only one choice for p_3 with p_2 above the x-axis. Similarly, when leaving $\mathcal{A}$, there is only one choice for p_3 with p_2 below the x-axis. Thus there are exactly two distinct paths between $\mathcal{A}$ and $\mathcal{C}$ (see Figure 3.19).

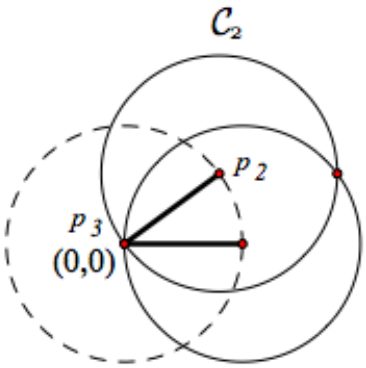

Figure 3.20: Moving from $\mathcal{B}$ to $\mathcal{C}$ with p_2 above the x-axis and p_3 fixed at $(0,0)$.

Now start at $\mathcal{B}$. As p_2 moves from $(s,0)$ to $(-s,0)$ along $\mathcal{C}_1$, it can move either above or below the x-axis. In either case, p_3 starts at $(0,0)$ and remains fixed the whole time (see Figure 3.20). Thus there are exactly two distinct paths from $\mathcal{B}$ to $\mathcal{C}$, both keeping p_3 fixed.

We have now shown that there are two distinct paths between any two straight-line configurations. Thus the moduli space is homeomorphic to three circles, each touching the other two circles in a single point, i.e., $(\mathcal{S}^1 \vee \mathcal{S}^1) \vee_2 \mathcal{S}^1$ (see Figure 3.21).

□

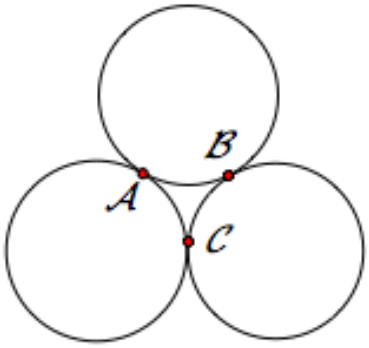

Figure 3.21: $M(s, s, s, s)$ is homeomorphic to three circles, each touching the other two circles once.

Chapter 4

Intraplanar Versus Extraplanar Motion

Now that we have reviewed the topology of $\mathcal{PM}(\vec{\ell})$ and $\mathcal{M}(\vec{\ell})$ we switch our focus to the geometry of these spaces, which is not well-studied. In studying the topology of these spaces we had Theorem 2.3.1 at our disposal, allowing us to rearrange the side lengths in a convenient order. As we transition to studying the geometry, we now have to consider the order in which the side lengths occur in $\vec{\ell}$. We can no longer shuffle the order around at our convenience. Our first approach to the geometry is dependent on the order of the side lengths.

4.1 Motivating Application

We start by describing a robotics application that motivates our first result: Suppose we are interested in the motion of a robot arm, where the first three segments of the arm have lengths ℓ_1, ℓ_2 and ℓ_3. Suppose the end of the arm is used to move an object along the positive x-axis. The position of this object on the positive x-axis determines the length of the fourth side of a quadrilateral, ℓ_4.

This larger space, where ℓ_4 is allowed to vary, is called the *space of arms* [10]. There is a map, called the *endpoint map*, which takes a point in the space of arms to the positive x-coordinate of the fourth side. In other words, the endpoint map records the position of the object being moved by the robot arm.

We are interested in analyzing the motion of this robot arm for a fixed position of the object. That is, we wish to study the geometry of a pre-image under the endpoint map. In particular, we are interested in comparing motion of the robot arm moving within the plane to motion of the robot arm moving out of the plane (with the end of the arm remaining fixed).

4.2 Formal Set-Up

Let $\vec{\ell} = (\ell_1, \ell_2, \ell_3, \ell_4)$ be given side lengths. Note that we no longer assume that ℓ_4 is the longest side.

Assumption 4.2.1. Given $\vec{\ell} = (\ell_1, \ell_2, \ell_3, \ell_4)$, suppose the side lengths $\ell_1, \ell_2 + \ell_3$, and ℓ_4

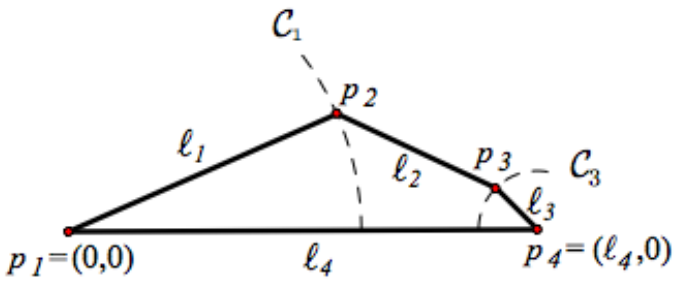

Figure 4.1: The point p_2 lies on circle $\mathcal{C}_1$ and the point p_3 lies on circle $\mathcal{C}_3$.

satisfy the strict triangle inequality: that is, the longest of the three is strictly less than the sum of the other two.

Remark 4.2.2. Note that Assumption 4.2.1 means that $\mathbf{x}_2$ and $\mathbf{x}_3$ can be straightened to form a non-degenerate triangle.

Remark 4.2.3. Alternatively we could have assumed that the side lengths $\ell_1 + \ell_2, \ell_3$, and ℓ_4 satisfy the strict triangle inequality, and hence $\mathbf{x}_1$ and $\mathbf{x}_2$ could be straightened to form a non-degenerate triangle. The geometry would remain unchanged but the specific formulas and illustrations would be slightly different.

Recall that we let $p_1 = (0, 0)$, $p_2 = (a, b)$ be the head of $\mathbf{x}_1$, $p_3 = (c, d)$ be the head of $\mathbf{x}_1 + \mathbf{x}_2$, and $p_4 = (\ell_4, 0)$. The points p_1 and p_4 are fixed and the points p_2 and p_3 are free to move. Recall that p_2 can move along $\mathcal{C}_1$ and p_3 can move along $\mathcal{C}_3$ (see Figure 4.1).

For a fixed p_2, the choices for p_3 correspond to the intersection points of circles $\mathcal{C}_2$ and $\mathcal{C}_3$. Usually there are two points of intersection, call them p_3 and p_3' (see Figure 3.1), but

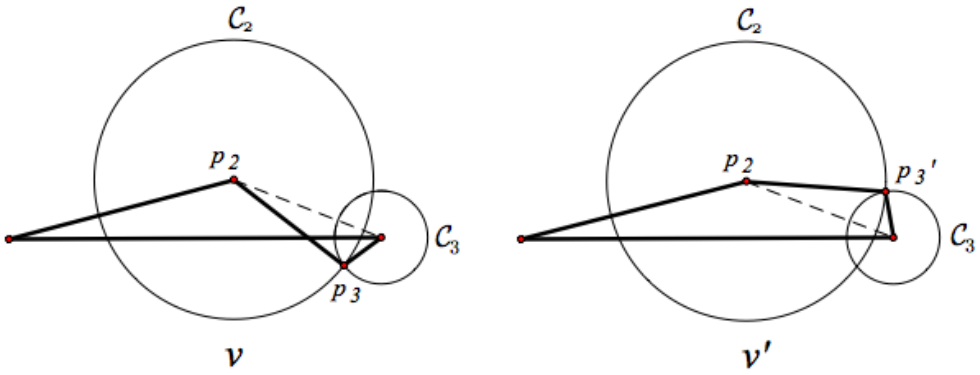

Figure 4.2: The quadrilaterals $\mathcal{V}$ and $\mathcal{V}'$.

occasionally there is only one point of intersection (if p_2 is at an endpoint of $\mathcal{W}^+$ or $\mathcal{W}^-$) or, in very special cases, infinitely many points of intersection (if $\mathcal{C}_2$ happens to be equal to $\mathcal{C}_3$).

We are interested in motion of the robot arm as it moves between configurations with the same p_2 but different p_3's. The two choices for p_3 can be viewed as a reflection across the line between p_2 and p_4.

Definition 4.2.4. For a fixed p_2 not at an endpoint of $\mathcal{W}$, let $\mathcal{V}$ be the quadrilateral with p_3 and $\mathcal{V}'$ be the quadrilateral with p_3' (see Figure 4.2).

We will examine paths between $\mathcal{V}$ and $\mathcal{V}'$. In particular, the robot arm can move through the $\triangle$-configuration and remain in the plane, or if we allow p_3 to leave the plane then p_2 can remain fixed while p_3 "swings out" along the circle of radius r (see Figure 4.3). We now examine the question: *Are there pairs of shapes, $\mathcal{V}$ and $\mathcal{V}'$, where it is shorter to move between them by remaining in the plane?*

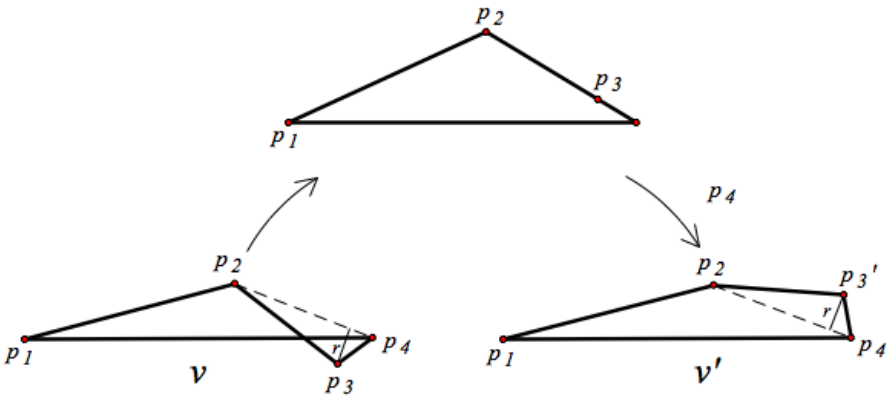

Figure 4.3: Moving in the plane through the $\triangle$-configuration, and p_3's circle of radius r.

4.2.1 Intraplanar Motion

Let $p_2 = (a(t), b(t))$ and $p_3 = (c(t), d(t))$ be parametrizations of the moving coordinates in the plane. Let $\mathbf{r}(t) = (a(t), b(t), c(t), d(t)) \in \mathbb{R}^4$ be a parametrization of the path in $\mathcal{M}(\vec{\ell})$ that begins at configuration $\mathcal{V}$, increases the angle p_2 makes with x-axis until it reaches the $\triangle$-configuration, then decreases p_2's angle and ends at configuration $\mathcal{V}'$, as illustrated in Figure 4.3.

Definition 4.2.5. Let $\mathbf{r}(t_0) = \mathcal{V}$ and $\mathbf{r}(t_1) = \mathcal{V}'$. Then define the Euclidean distance in $\mathbb{R}^4$ between $\mathcal{V}$ and $\mathcal{V}'$ to be

$$\text{EuclDistIn}(\mathcal{V}, \mathcal{V}') = \int_{t_0}^{t_1} \|\mathbf{r}'(t)\|\, dt = \int_{t_0}^{t_1} \sqrt{a'(t)^2 + b'(t)^2 + c'(t)^2 + d'(t)^2}\, dt$$

4.2.2 Extraplanar Motion

Let $p_2 = (a_0, b_0, 0)$ be the fixed point and $p_3 = (c(t), d(t), h(t))$ be a parametrization of p_3 as it swings out of the plane along the circle of radius r. Let $\mathbf{r}(t) = (a_0, b_0, 0, c(t), d(t), h(t)) \in \mathbb{R}^6$.

Definition 4.2.6. Let $\mathbf{r}(t_0) = \mathcal{V}$ and $\mathbf{r}(t_1) = \mathcal{V}'$. Then define the Euclidean distance in $\mathbb{R}^6$ between $\mathcal{V}$ and $\mathcal{V}'$ to be

$$\text{EuclDistOut}(\mathcal{V}, \mathcal{V}') = \int_{t_0}^{t_1} \|\mathbf{r}'(t)\|\, dt = \int_{t_0}^{t_1} \sqrt{c'(t)^2 + d'(t)^2 + h'(t)^2}\, dt$$

Observe that $\text{EuclDistOut}(\mathcal{V}, \mathcal{V}')$ is half the circumference of a circle with radius r.

4.3 Intraplanar Versus Extraplanar Motion

Theorem 4.3.1. *Given $\vec{\ell}$ satisfying Assumption 4.2.1, there is a neighborhood of the $\triangle$-configuration where, for $\mathcal{V}$ and $\mathcal{V}'$ in that neighborhood,* $\text{EuclDistIn}(\mathcal{V}, \mathcal{V}') < \text{EuclDistOut}(\mathcal{V}, \mathcal{V}')$.

Remark 4.3.2. The focus on comparing the distance between configurations $\mathcal{V}$ and $\mathcal{V}'$ near the $\triangle$-configuration is motivated by calculations in Mathematica where $\vec{\ell} = (5, 3, 1, \ell_4)$, with $7 < \ell_4 < 9$. These calculations indicated that away from the $\triangle$-configuration it was shorter to leave the plane. The interesting observation from these calculations was that there was always a small neighborhood of the $\triangle$-configuration where it was faster to remain in the plane, and this is why we focused on this result. We have not yet identified the conditions under which it is shorter to leave the plane.

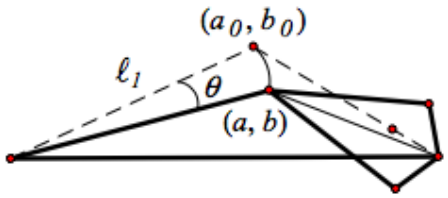

Figure 4.4: The angle θ.

Before proving the theorem we introduce a tool we use in the analysis and give an intuition for the proof. The tool we introduce is an alternate way to measure the distance between $\mathcal{V}$ and $\mathcal{V}'$ that has a convenient relationship to EuclDistIn and EuclDistOut.

4.3.1 Tool In The Analysis

Because both p_2 and p_3 move along arcs of circles, we may easily calculate the distance each point travels separately and add the results to get a new measure of distance.

Let (a_0, b_0) be the coordinates of p_2 at the $\triangle$-configuration and (a, b) be the coordinates of p_2 at $\mathcal{V}$. Let θ be the angle measured counterclockwise from $< a, b >$ to $< a_0, b_0 >$, as shown in Figure 4.4. In moving from $\mathcal{V}$ to $\mathcal{V}'$, the point p_2 moves along $\mathcal{C}_1$ up to the $\triangle$-configuration and then back down to its starting position. Thus p_2 travels a total distance of $2\ell_1\theta$.

Let (c, d) be the coordinates of p_3 at shape $\mathcal{V}$ and let (c', d') be the coordinates of p'_3 at shape $\mathcal{V}'$. Let α be the angle measured clockwise from the vector $< c - \ell_4, d >$ to the line between p_2 and p_4, as shown in Figure 4.5. Note that, for p'_3 at shape $\mathcal{V}'$, the angle measured

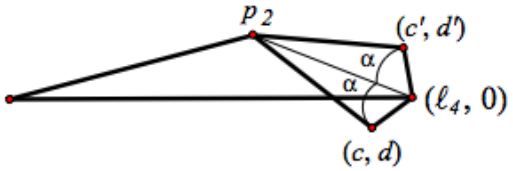

Figure 4.5: The angle α.

clockwise from the line between p_2 and p_4 to vector $< c' - \ell_4, d' >$ is also α. Thus p_3 travels a total distance of $2\ell_3\alpha$.

Definition 4.3.3. Define the intraplanar distance between $\mathcal{V}$ and $\mathcal{V}'$ using this new measure to be

$$\text{DistIn}(\mathcal{V}, \mathcal{V}') = 2\ell_1\theta + 2\ell_3\alpha$$

If p_2 remains fixed and p_3 moves out of the plane along the circle of radius $r = \ell_3 \sin(\alpha)$, the point p_3 travels half the circumference of that circle. Thus p_3's total distance traveled is $\pi\ell_3 \sin(\alpha)$ and p_2's distance traveled is zero.

Notation 4.3.4. Let the extraplanar distance between $\mathcal{V}$ and $\mathcal{V}'$ be denoted by

$$\text{DistOut}(\mathcal{V}, \mathcal{V}') = \pi\ell_3 \sin(\alpha)$$

Note: $\text{DistOut}(\mathcal{V}, \mathcal{V}') = \text{EuclDistOut}(\mathcal{V}, \mathcal{V}')$.

Lemma 4.3.5. *Suppose there is a neighborhood of the $\triangle$-configuration where, for $\mathcal{V}$ and $\mathcal{V}'$ in that neighborhood,* $\text{DistIn}(\mathcal{V}, \mathcal{V}') < \text{DistOut}(\mathcal{V}, \mathcal{V}')$. *Then for $\mathcal{V}$ and $\mathcal{V}'$ in that neighborhood,* $\text{EuclDistIn}(\mathcal{V}, \mathcal{V}') < \text{EuclDistOut}(\mathcal{V}, \mathcal{V}')$.

Proof.

$$\begin{aligned}
\text{EuclDistIn}(\mathcal{V}, \mathcal{V}') &= \int_{t_0}^{t_1} \sqrt{a'(t)^2 + b'(t)^2 + c'(t)^2 + d'(t)^2}\, dt \\
&\leq \int_{t_0}^{t_1} \sqrt{a'(t)^2 + b'(t)^2}\, dt + \int_{t_0}^{t_1} \sqrt{c'(t)^2 + d'(t)^2}\, dt \\
&= \text{DistIn}(\mathcal{V}, \mathcal{V}') \\
&< \text{DistOut}(\mathcal{V}, \mathcal{V}') \\
&= \text{EuclDistOut}(\mathcal{V}, \mathcal{V}')
\end{aligned}$$

□

Therefore, in order to prove Theorem 4.3.1, it suffices to show that there is a neighborhood of the $\triangle$-configuration where, for $\mathcal{V}$ and $\mathcal{V}'$ in that neighborhood, $\text{DistIn}(\mathcal{V}, \mathcal{V}') < \text{DistOut}(\mathcal{V}, \mathcal{V}')$.

4.3.2 Intuition For The Proof

Both θ and α increase as we move away from the $\triangle$-configuration, so we must compare their relative rates of change. The angle α grows faster than θ moving away from the $\triangle$-configuration, so θ is smaller than α near the $\triangle$-configuration. Then for α near zero, $\theta \approx 0$. Also, for α near zero, $\sin(\alpha) \approx \alpha$. Thus for α near zero, $\text{DistIn}(\mathcal{V}, \mathcal{V}') \approx 2\ell_3\alpha$ is less than $\text{DistOut}(\mathcal{V}, \mathcal{V}') \approx \pi\ell_3\alpha$.

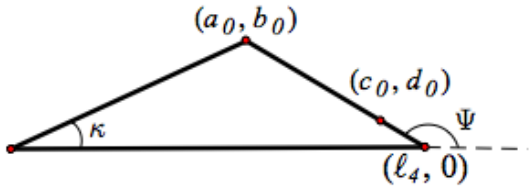

Figure 4.6: The coordinates at the $\triangle$-configuration.

4.3.3 Proof of Theorem 4.3.1

Proof. Let

$$\begin{aligned} a_0 &= \ell_1 \cos(\kappa) \\ b_0 &= \ell_1 \sin(\kappa) \\ c_0 &= \ell_4 + \ell_3 \cos(\Psi) \\ d_0 &= \ell_3 \sin(\Psi) \end{aligned}$$

be the coordinates at the $\triangle$-configuration, as shown in Figure 4.6.

Let

$$\begin{aligned} a &= \ell_1 \cos(\kappa - \theta) \\ b &= \ell_1 \sin(\kappa - \theta) \\ c &= \ell_4 + \ell_3 \cos(\Psi - \beta) \\ d &= \ell_3 \sin(\Psi - \beta) \end{aligned}$$

be the general coordinates of p_2 and p_3, as shown in Figure 4.7. Let θ be the angle measured

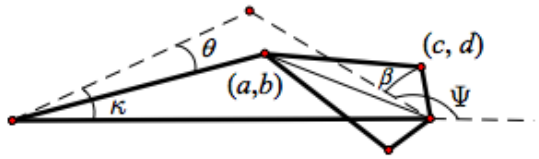

Figure 4.7: General coordinates for p_2 and p_3 and the angles θ and β, both positive.

counterclockwise from $< a, b >$ to $< a_0, b_0 >$ and let β be the angle measured clockwise from $< c_0 - \ell_4, d_0 >$ to $< c - \ell_4, d >$ (see Figure 4.7).

Claim 4.3.6. *Viewing θ as a function of β, we claim that $\dfrac{d\theta}{d\beta} \to 0$ as $\beta \to 0$.*

We first use Claim 4.3.6 to show that, for α near 0,

$$\text{DistOut}(\mathcal{V}, \mathcal{V}') - \text{DistIn}(\mathcal{V}, \mathcal{V}') = \pi\ell_3 \sin(\alpha) - (2\ell_1\theta + 2\ell_3\alpha) > 0 \tag{4.1}$$

After showing Equation (4.1) is true we will prove Claim 4.3.6.

Let $f(\theta) = -2\ell_1\theta$ and $g(\alpha) = \pi\ell_3 \sin(\alpha) - 2\ell_3\alpha$. We want to show $f(\theta) + g(\alpha) > 0$ for α near 0. By the Mean Value Theorem,

$$\begin{aligned} f(\theta) &= \frac{df}{d\theta}(\tilde{\theta})\theta \\ g(\alpha) &= \frac{dg}{d\alpha}(\tilde{\alpha})\alpha \\ \theta(\beta) &= \frac{d\theta}{d\beta}(\tilde{\beta})\beta \end{aligned}$$

for some $\tilde{\theta}, \tilde{\alpha}, \tilde{\beta}$ all near zero. Note that $\beta \leq 2\alpha$ for α small. Then

$$\begin{aligned} f(\theta) + g(\alpha) &= \frac{df}{d\theta}(\tilde{\theta})\theta(\beta) + \frac{dg}{d\alpha}(\tilde{\alpha})\alpha \\ &= \frac{df}{d\theta}(\tilde{\theta})\frac{d\theta}{d\beta}(\tilde{\beta})\beta + \frac{dg}{d\alpha}(\tilde{\alpha})\alpha \\ &= -2\ell_1\frac{d\theta}{d\beta}(\tilde{\beta})\beta + (\pi\ell_3\cos(\tilde{\alpha}) - 2\ell_3)\alpha \\ &\geq -2\ell_1\frac{d\theta}{d\beta}(\tilde{\beta})2\alpha + (\pi\ell_3\cos(\tilde{\alpha}) - 2\ell_3)\alpha \\ &= \left(-4\ell_1\frac{d\theta}{d\beta}(\tilde{\beta}) + \pi\ell_3\cos(\tilde{\alpha}) - 2\ell_3\right)\alpha \end{aligned}$$

Note that $\beta \to 0$ as $\alpha \to 0$. Therefore $\dfrac{d\theta}{d\beta}(\tilde{\beta}) \to 0$ and $\cos(\tilde{\alpha}) \to 1$ as $\alpha \to 0$. Thus $f(\theta) + g(\alpha)$ is greater than or equal to something approaching $(0 + \pi\ell_3 - 2\ell_3)\alpha$ as $\alpha \to 0$. Because $\pi\ell_3 - 2\ell_3 > 0$, $f(\theta) + g(\alpha) > 0$ for α near zero. Therefore Equation (4.1) is true for α near zero.

Now we prove Claim 4.3.6:

First observe that we have the following relationship between θ and the coordinates of p_2 in general and the coordinates of p_2 at the $\triangle$-configuration:

$$\ell_1^2\cos(\theta) = a_0 a + b_0 b$$

By differentiating $\ell_1^2\cos(\theta) = a_0 a + b_0 b$ with respect to β, we have

$$\ell_1^2(-\sin(\theta))\frac{d\theta}{d\beta} = a_0\frac{da}{d\beta} + b_0\frac{db}{d\beta} \tag{4.2}$$

Our goal is to show that $\dfrac{d\theta}{d\beta}$ behaves like a term on the right-hand side of Equation (4.2) that goes to zero as β goes to zero.

To achieve this we first show that $\frac{da}{d\beta}$ and $\frac{db}{d\beta}$ can be written in terms of $\frac{dc}{d\beta}$ and $\frac{dd}{d\beta}$. This is desirable because, since $c = \ell_4 + \ell_3 \cos(\Psi - \beta)$ and $d = \ell_3 \sin(\Psi - \beta)$, both $\frac{dc}{d\beta}$ and $\frac{dd}{d\beta}$ can be calculated directly.

To do this we differentiate the equations of circles $\mathcal{C}_1$ and $\mathcal{C}_2$,

$$\begin{aligned} a^2 + b^2 &= \ell_1^2 \\ (c-a)^2 + (d-b)^2 &= \ell_2^2 \end{aligned}$$

with respect to β to get the following system of equations:

$$\begin{aligned} 2a\frac{da}{d\beta} + 2b\frac{db}{d\beta} &= 0 \\ 2(c-a)\left(\frac{dc}{d\beta} - \frac{da}{d\beta}\right) + 2(d-b)\left(\frac{dd}{d\beta} - \frac{db}{d\beta}\right) &= 0 \end{aligned}$$

We now solve this system of equations for $\frac{da}{d\beta}$ and $\frac{db}{d\beta}$. To simplify the notation a little bit, let

$$\begin{aligned} x &= 2a \\ y &= 2b \\ z &= 2(c-a) \\ w &= 2(d-b) \\ v &= 2(c-a)\frac{dc}{d\beta} + 2(d-b)\frac{dd}{d\beta} \end{aligned}$$

Solving for $\frac{da}{d\beta}$ and $\frac{db}{d\beta}$ gives $\frac{da}{d\beta} = -\frac{vy}{xw - zy}$ and $\frac{db}{d\beta} = \frac{xv}{xw - zy}$, so long as $xw - zy$ is bounded away from zero.

To see that $xw - zy$ is bounded away from zero (for β near zero), note that $xw - zy = 4a(d-b) - 4b(c-a) = 0$ if and only if

$$\begin{vmatrix} a & b \\ (c-a) & (d-b) \end{vmatrix} = 0 \tag{4.3}$$

Equation (4.3) is true if and only if $\mathbf{x}_1$ and $\mathbf{x}_2$ are collinear. In the limit as $\beta \to 0$, $xw - zy \to 4a_0(d_0 - b_0) - 4b_0(c_0 - a_0)$, which equals zero if and only if $\mathbf{x}_1, \mathbf{x}_2$ and $\mathbf{x}_3$ are all collinear at the $\triangle$-configuration. But we have assumed that this does not happen because the $\triangle$-configuration is non-degenerate. Therefore $4a_0(d_0 - b_0) - 4b_0(c_0 - a_0)$ is bounded away from zero, and in a neighborhood of the $\triangle$-configuration, $xw - zy$ is bounded away from zero.

We can now rewrite Equation (4.2) as:

$$\begin{aligned} \ell_1^2(-\sin(\theta))\frac{d\theta}{d\beta} &= a_0\frac{da}{d\beta} + b_0\frac{db}{d\beta} \\ &= \frac{-a_0vy + b_0xv}{xw - zy} \\ &= v\left(\frac{-a_0y + b_0x}{xw - zy}\right) \\ &= v\left(\frac{-a_02b + b_02a}{xw - zy}\right) \end{aligned}$$

Because $xw - zy$ is bounded away from zero in a neighborhood of the $\triangle$-configuration, $\ell_1^2(-\sin(\theta))\frac{d\theta}{d\beta} \sim v(-a_02b + b_02a)$, where the symbol "$\sim$" means "decays like" in the limit. Observe that $-a_02b + b_02a \to 0$ as $\beta \to 0$.

Next we show that $-a_02b + b_02a$ decays like θ, and then because $\sin(\theta)$ decays like θ we will have shown that $\dfrac{d\theta}{d\beta}$ decays like v. All that will be left to show after that is that v goes to

zero as β goes to zero.

We now wish to write $-a_0 2b + b_0 2a$ as a series in θ. First, observe that $-a_0 2b + b_0 2a = -2\ell_1 a_0 \sin(\kappa - \theta) + 2\ell_1 b_0 \cos(\kappa - \theta)$. The Taylor Series expansion in θ for $\sin(\kappa - \theta)$ and $\cos(\kappa - \theta)$ is:

$$\begin{aligned} \sin(\kappa - \theta) &= \sin(\kappa) + \eta_1\theta + \eta_2\theta^2 + \dots \text{ and} \\ \cos(\kappa - \theta) &= \cos(\kappa) + \gamma_1\theta + \gamma_2\theta^2 + \dots \end{aligned}$$

respectively. Now observe that the constant term in $-a_0 2b + b_0 2a$ is $-2\ell_1^2 \cos(\kappa)\sin(\kappa) + 2\ell_1^2 \sin(\kappa)\cos(\kappa) = 0$. Therefore $-a_0 2b + b_0 2a$ decays like θ.

Finally we show that $v \to 0$ as $\beta \to 0$. Observe that $\dfrac{dc}{d\beta} = \ell_3 \sin(\Psi - \beta)$ and $\dfrac{dd}{d\beta} = -\ell_3 \cos(\Psi - \beta)$. Then

$$\begin{aligned} v &= 2(c-a)\frac{dc}{d\beta} + 2(d-b)\frac{dd}{d\beta} \\ &= 2(c-a)\ell_3 \sin(\Psi - \beta) + 2(d-b)(-\ell_3)\cos(\Psi - \beta) \end{aligned}$$

As $\beta \to 0$, $v \to 2(c_0 - a_0)\ell_3 \sin(\Psi) - 2(d_0 - b_0)\ell_3 \cos(\Psi)$ which equals zero by right triangle geometry (see Figure 4.8) and the observation that

$$\tan(\pi - \Psi) = \frac{b_0 - d_0}{c_0 - a_0} = -\tan(\Psi)$$

Therefore $v \to 0$ as $\beta \to 0$ and hence $\dfrac{d\theta}{d\beta} \to 0$ as $\beta \to 0$ and Claim 4.3.6 is proved.

□

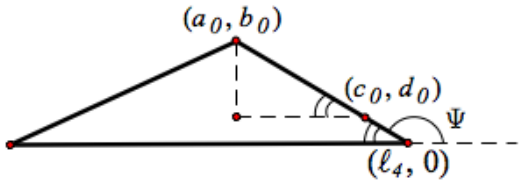

Figure 4.8: Right triangle geometry.

Notes on Assumption 4.2.1

1. The proof is analogous (mirror image) if $\mathbf{x}_1$ and $\mathbf{x}_2$ are straightened.

2. For the square and *some* rectangle cases the result does not hold because the $\triangle$-configuration is degenerate.

3. If $\mathbf{x}_2$ can't be straightened with an adjacent side then the proof fails. This can be addressed by a cyclic permutation of the side lengths, but doing so will change the physical distance measurements.

4.3.4 Corollary for the Degenerate Triangle Case

We now consider the case where the $\triangle$-configuration is degenerate. Note that this occurs if

$$\vec{\ell} \in \begin{cases} (s,l,s,l) \\ (l,s,l,s) \\ (l,l,s,s) \\ (s,l,l,s) \\ (s,s,s,s) \end{cases} \tag{4.4}$$

where $l, s > 0$ with $l > s$.

Note that there are two rectangle cases, $\vec{\ell} = (s,s,l,l)$ and $\vec{\ell} = (l,s,s,l)$, that *do* satisfy the conditions of Theorem 4.3.1. This is because the order of the side lengths is such that the two shortest sides are adjacent, one of them is in the ℓ_2 position, and therefore they can be straightened to form an isoceles triangle, which is non-degenerate.

However, for the five cases in (4.4), it is always shorter to use extraplanar motion when moving from $\mathcal{V}$ to $\mathcal{V}'$.

Corollary 4.3.7. *Suppose* $\vec{\ell} \in \{(s,l,s,l),(l,s,l,s),(l,l,s,s),(s,l,l,s),(s,s,s,s)\}$. *Then for any pair of quadrilaterals,* $\mathcal{V}$ *and* $\mathcal{V}'$, $\mathrm{DistOut}(\mathcal{V},\mathcal{V}') < \mathrm{DistIn}(\mathcal{V},\mathcal{V}')$.

Proof. There are five cases to consider:

(a) $\vec{\ell} = (s,l,s,l)$

(b) $\vec{\ell} = (l, s, l, s)$

(c) $\vec{\ell} = (l, l, s, s)$

(d) $\vec{\ell} = (s, l, l, s)$

(e) $\vec{\ell} = (s, s, s, s)$

We will start by proving (a), then note that the proof of (b) is the same as the proof of (a) where "s" is replaced with "l". Then we will prove (c) and note that the proof of (d) is just the mirror image of (c). Finally, we will show that the proof of (e) is just a special case of the proof of (a).

Case (a): $\vec{\ell} = (s, l, s, l)$

In this case $\mathbf{x}_2$ may be straightened with either $\mathbf{x}_1$ or $\mathbf{x}_3$, both forming a degenerate quadrilateral. For purposes of illustration we choose to straighten $\mathbf{x}_2$ and $\mathbf{x}_3$.

With $\mathbf{x}_2$ and $\mathbf{x}_3$ straightened, the degenerate $\triangle$-configuration is the shape with $p_2 = (-s, 0)$ and $p_3 = (l - s, 0)$. Let θ and α be the angles shown in Figure 4.9. It is clear from Figure 4.9 that $\theta \geq \alpha$.

Then

$$\begin{aligned} \text{DistIn}(\mathcal{V}, \mathcal{V}') &= 2s\theta + 2s\alpha, \text{ and} \\ \text{DistOut}(\mathcal{V}, \mathcal{V}') &= \pi s \sin(\alpha) \end{aligned}$$

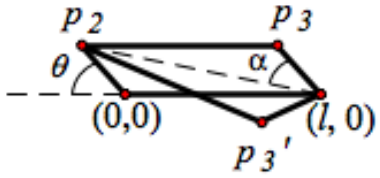

Figure 4.9: Set-up for Case (a): $\vec{\ell} = (s, l, s, l)$.

Thus

$$\begin{aligned} \text{DistIn}(\mathcal{V}, \mathcal{V}') &= 2s\theta + 2s\alpha \\ &\geq 4s\alpha \text{ (since } \theta \geq \alpha) \\ &> \pi s\alpha \\ &\geq \pi s \sin(\alpha) \\ &= \text{DistOut}(\mathcal{V}, \mathcal{V}') \end{aligned}$$

Case (b): $\vec{\ell} = (l, s, l, s)$

Simply replace "s" with "l" in the proof above to get the same result.

Case (c): $\vec{\ell} = (l, l, s, s)$

In this case only $\mathbf{x}_2$ and $\mathbf{x}_3$ can be straightened to form the degenerate $\triangle$-configuration. At this configuration we have $p_2 = (-l, 0)$ and $p_3 = (0, 0)$. Let θ and α be the angles shown in Figure 4.10. It is clear from Figure 4.10 that $\theta \geq \alpha$.

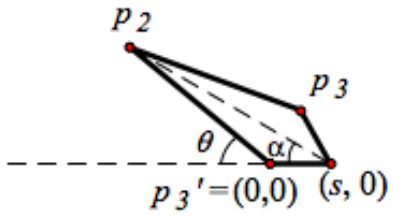

Figure 4.10: Set-up for Case (c): $\vec{\ell} = (l, l, s, s)$.

Then

$$\begin{aligned} \text{DistIn}(\mathcal{V}, \mathcal{V}') &= 2l\theta + 2s\alpha \\ \text{DistOut}(\mathcal{V}, \mathcal{V}') &= \pi s \sin(\alpha) \end{aligned}$$

Thus

$$\begin{aligned} \text{DistIn}(\mathcal{V}, \mathcal{V}') &= 2l\theta + 2s\alpha \\ &\geq 2l\alpha + 2s\alpha \text{ (since } \theta \geq \alpha) \\ &> 4s\alpha \\ &> \pi s\alpha \\ &\geq \pi s \sin(\alpha) \\ &= \text{DistOut}(\mathcal{V}, \mathcal{V}') \end{aligned}$$

Case (d): $\vec{\ell} = (s, l, l, s)$

In this case only $\mathbf{x}_1$ and $\mathbf{x}_2$ can be straightened to form the degenerate $\triangle$-configuration. The set-up and proof of this case is the mirror image of the set-up and proof for Case (c).

Case (e): $\vec{\ell} = (s, s, s, s)$

The proof of the square case is just a special case of the proof of (a), with $l = s$. Because l does not appear in either distance formula for Case (a), the same distance formulas apply in Case (e) and the proof is the same.

□

4.4 A Vector-Based Distance

Previously we defined our distances based on the two vertices that are free to move: p_2 and p_3. It is worth noting that we could also define distances based on the three vectors that are free to move: $\mathbf{x}_1$, $\mathbf{x}_2$, and $\mathbf{x}_3$. We will define these new distances and show that we can recover the result of Theorem 4.3.1.

Recall that $\mathbf{x}_1 = p_2, \mathbf{x}_2 = p_3 - p_2$, and $\mathbf{x}_3 = p_4 - p_3$, where $p_4 = (\ell_4, 0)$ is fixed. For intraplanar motion between $\mathcal{V}$ and $\mathcal{V}'$, all three vectors move. For extraplanar motion between $\mathcal{V}$ and $\mathcal{V}'$, only $\mathbf{x}_2$ and $\mathbf{x}_3$ move.

4.4.1 Intraplanar Motion

Let $\mathbf{r}(t) = (a(t), b(t), c(t) - a(t), d(t) - b(t), \ell_4 - c(t), -d(t)) = (p_2(t), p_3(t) - p_2(t), p_4 - p_3(t))$ be a parametrization of the path in $\mathcal{M}(\vec{\ell})$ that begins at configuration $\mathcal{V}$, increases the angle p_2 makes with x-axis until it reaches the $\triangle$-configuration, then decreases p_2's angle and ends

at configuration $\mathcal{V}'$, as illustrated in Figure 4.3.

Definition 4.4.1. Let $\mathbf{r}(t_0) = \mathcal{V}$ and $\mathbf{r}(t_1) = \mathcal{V}'$. Then define the vector Euclidean distance in $\mathbb{R}^6$ between $\mathcal{V}$ and $\mathcal{V}'$ to be

$$\begin{aligned}
\text{VecEuclDistIn}(\mathcal{V}, \mathcal{V}') &= \int_{t_0}^{t_1} \|\mathbf{r}'(t)\|\, dt \\
&= \int_{t_0}^{t_1} \sqrt{p_2' \cdot p_2' + (p_3' - p_2') \cdot (p_3' - p_2') + p_3' \cdot p_3'}\, dt \\
&= \int_{t_0}^{t_1} \sqrt{2p_2' \cdot p_2' + 2p_3' \cdot p_3' - 2p_2' \cdot p_3'}\, dt \\
&= \sqrt{2} \int_{t_0}^{t_1} \sqrt{p_2' \cdot p_2' + p_3' \cdot p_3' - (p_2' \cdot p_3')}\, dt
\end{aligned}$$

4.4.2 Extraplanar Motion

Now we define the distance on vectors $\mathbf{x}_2$ and $\mathbf{x}_3$ as they swing out of the plane. Note that the base of $\mathbf{x}_2$ (which is the point $(a_0, b_0, 0)$) is fixed and only the head (which is the point (c, d, h)) moves. Similarly, the tail of $\mathbf{x}_3$ (which is also the point (c, d, h)) moves while the head (which is the point $(\ell_4, 0, 0)$) stays fixed. Let $\mathbf{r}(t) = (c(t) - a_0, d(t) - b_0, h(t), \ell_4 - c(t), -d(t), -h(t))$ be a parametrization of the coordinates of $\mathbf{x}_2$ and $\mathbf{x}_3$.

Definition 4.4.2. Let $\mathbf{r}(t_0) = \mathcal{V}$ and $\mathbf{r}(t_1) = \mathcal{V}'$. Then define the vector Euclidean distance in $\mathbb{R}^6$ moving out of the plane between $\mathcal{V}$ and $\mathcal{V}'$ to be

$$\begin{aligned}
\text{VecEuclDistOut}(\mathcal{V}, \mathcal{V}') &= \int_{t_0}^{t_1} \|\mathbf{r}'(t)\|\, dt \\
&= \int_{t_0}^{t_1} \sqrt{2(c')^2 + 2(d')^2 + 2(h')^2}\, dt \\
&= \sqrt{2} \int_{t_0}^{t_1} \sqrt{(c')^2 + (d')^2 + (h')^2}\, dt
\end{aligned}$$

Also note that

$$\text{VecEuclDistOut}(\mathcal{V}, \mathcal{V}') = \sqrt{2}\,\text{EuclDistOut}(\mathcal{V}, \mathcal{V}') = \sqrt{2}\pi\ell_3 \sin(\alpha) \tag{4.5}$$

4.4.3 Comparisons Near The $\triangle$-configuration

Assume we have a pair of shapes, $\mathcal{V}$ and $\mathcal{V}'$, near the $\triangle$-configuration. We will show that, for α near zero, $\text{VecEuclDistIn}(\mathcal{V}, \mathcal{V}') < \text{VecEuclDistOut}(\mathcal{V}, \mathcal{V}')$.

First we need the following Lemma:

Lemma 4.4.3. $\text{VecEuclDistIn}(\mathcal{V}, \mathcal{V}') \leq 2\,\text{EuclDistIn}(\mathcal{V}, \mathcal{V}')$

Proof.

$$\begin{aligned}
\text{VecEuclDistIn}(\mathcal{V}, \mathcal{V}') &= \sqrt{2}\int_{t_0}^{t_1} \sqrt{p_2' \cdot p_2' + p_3' \cdot p_3' - (p_2' \cdot p_3')}\, dt \\
&\leq \sqrt{2}\int_{t_0}^{t_1} \sqrt{p_2' \cdot p_2' + p_3' \cdot p_3' + |p_2' \cdot p_3'|}\, dt \\
&\leq \sqrt{2}\int_{t_0}^{t_1} \sqrt{p_2' \cdot p_2' + p_3' \cdot p_3' + \|p_2'\|\|p_3'\|}\, dt \\
&\leq \sqrt{2}\int_{t_0}^{t_1} \sqrt{p_2' \cdot p_2' + p_3' \cdot p_3' + (\max\{\|p_2'\|, \|p_3'\|\})^2}\, dt \\
&\leq \sqrt{2}\int_{t_0}^{t_1} \sqrt{p_2' \cdot p_2' + p_3' \cdot p_3' + \|p_2'\|^2 + \|p_3'\|^2}\, dt \\
&= \sqrt{2}\int_{t_0}^{t_1} \sqrt{p_2' \cdot p_2' + p_3' \cdot p_3' + p_2' \cdot p_2' + p_3' \cdot p_3'}\, dt \\
&= 2\int_{t_0}^{t_1} \sqrt{p_2' \cdot p_2' + p_3' \cdot p_3'}\, dt \\
&= 2\int_{t_0}^{t_1} \sqrt{(a')^2 + (b')^2 + (c')^2 + (d')^2}\, dt \\
&= 2\,\text{EuclDistIn}(\mathcal{V}, \mathcal{V}')
\end{aligned}$$

□

Theorem 4.4.4. *For $\vec{\ell}$ satisfing Assumption 4.2.1 there is a neighborhood of the $\triangle$-configuration where, for $\mathcal{V}$ and $\mathcal{V}'$ in that neighborhood,* $\text{VecEuclDistIn}(\mathcal{V}, \mathcal{V}') < \text{VecEuclDistOut}(\mathcal{V}, \mathcal{V}')$.

Proof. We use the same set-up for the proof as shown in Figure 4.7.

$$\begin{aligned}
\text{VecEuclDistOut}(\mathcal{V}, \mathcal{V}') - \text{VecEuclDistIn}(\mathcal{V}, \mathcal{V}') &= \sqrt{2}\,\text{EuclDistOut} - \text{VecEuclDistIn}(\mathcal{V}, \mathcal{V}') \\
&= \sqrt{2}\pi\ell_3 \sin(\alpha) - \text{VecEuclDistIn}(\mathcal{V}, \mathcal{V}') \\
&\geq \sqrt{2}\pi\ell_3 \sin(\alpha) - 2\,\text{EuclDistIn}(\mathcal{V}, \mathcal{V}') \text{ (Lemma 4.4.3)} \\
&\geq \sqrt{2}\pi\ell_3 \sin(\alpha) - 2\,\text{DistIn}(\mathcal{V}, \mathcal{V}') \\
&= \sqrt{2}\pi\ell_3 \sin(\alpha) - 2(2\ell_1\theta + 2\ell_3\alpha) \\
&= \sqrt{2}(\pi\ell_3 \sin(\alpha) - 2\sqrt{2}(\ell_1\theta + \ell_3\alpha))
\end{aligned}$$

Let $f(\theta) = -2\sqrt{2}\ell_1\theta$ and $g(\alpha) = \pi\ell_3 \sin(\alpha) - 2\sqrt{2}\ell_3\alpha$. Using the Mean Value Theorem, as in the proof of Theorem 4.3.1, we may write

$$f(\theta) + g(\alpha) = -2\sqrt{2}\ell_1 \frac{d\theta}{d\beta}(\tilde{\beta})\beta + (\pi\ell_3 \cos(\alpha) - 2\sqrt{2}\ell_3)\alpha$$

for some $\tilde{\beta}$ near zero. Also recall that $\beta \leq 2\alpha$ for α near zero. Then

$$\begin{aligned}
f(\theta) + g(\alpha) &= -2\sqrt{2}\ell_1 \frac{d\theta}{d\beta}(\tilde{\beta})\beta + (\pi\ell_3 \cos(\alpha) - 2\sqrt{2}\ell_3)\alpha \\
&\leq \left(-4\sqrt{2}\ell_1 \frac{d\theta}{d\beta}(\tilde{\beta}) + (\pi\ell_3 \cos(\alpha) - 2\sqrt{2}\ell_3)\right)\alpha
\end{aligned}$$

As $\alpha \to 0$, $\beta \to 0$ and hence $\dfrac{d\theta}{d\beta} \to 0$. Then $f(\theta) + g(\alpha) \to 0 + \ell_3(\pi - 2\sqrt{2}) > 0$.

Therefore, for α near zero,

$$\text{VecEuclDistOut}(\mathcal{V}, \mathcal{V}') - \text{VecEuclDistIn}(\mathcal{V}, \mathcal{V}') \quad \geq \quad \sqrt{2}(f(\theta) + g(\alpha))$$

and $f(\theta) + g(\alpha) > 0$.

Thus, $\text{VecEuclDistIn}(\mathcal{V}, \mathcal{V}') < \text{VecEuclDistOut}(\mathcal{V}, \mathcal{V}')$ for α near zero.

□

4.5 Problems With This Approach

The main problem with defining distances on either the moving vectors or vertices is that it requires fixing ℓ_4. The distances themselves also depend on the order in which ℓ_1, ℓ_2 and ℓ_3 appear. Thus neither distance is invariant under permutations of side lengths.

If one is working in the context of the robot arm example, then this problem may not be relevant. However, in general, we would like to be able to define a distance that is invariant under side length permutations because the goal is to study the geometry of spaces of quadrilaterals. For example, we would like the distance between the shapes in Figure 4.11 to be the same as the distance between the shapes in Figure 4.12.

We have been working in the context of Equation (2.1), where ℓ_4 is fixed along the positive x-axis. We must now put aside this representation of $\mathcal{M}(\vec{\ell})$ and use a metric on $\mathcal{PM}(\vec{\ell})$ to get a better metric on $\mathcal{M}(\vec{\ell})$.

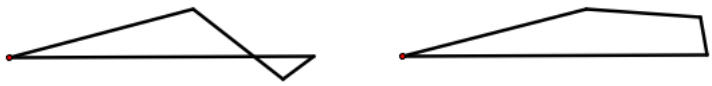

Figure 4.11: Two shapes in $\mathcal{M}(5, 3, 1, 8)$

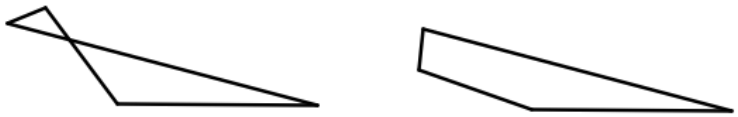

Figure 4.12: Two shapes in $\mathcal{M}(3, 1, 8, 5)$

Chapter 5

Geometry of Spaces of Planar Quadrilaterals

A good choice of distance (lengths of paths) on the moduli space should not depend on constrained choices of equivalence class representatives, as the Chapter 4 distance did when it was based on fixing the fourth side. One way to make such a choice is to define a Riemannian metric on the pre-moduli space that is invariant under the $SO(2)$ action. We will use a restriction of the Riemannian metric introduced by Kendall [7].

For two points $X, Y \in \mathcal{M}(\vec{\ell})$, the length of a path from X to Y in $\mathcal{M}(\vec{\ell})$ is defined to be the length of the shortest lift of that path from $\pi^{-1}(X)$ to $\pi^{-1}(Y)$ in $\mathcal{PM}(\vec{\ell})$. This shortest lift will be the lift whose tangent vectors are everywhere orthogonal to the $SO(2)$ orbits in the sense defined by the Riemannian metric. An interesting geometric phenomenon, holonomy,

can arise from these lifts of paths.

This Riemannian metric (and hence the metric it induces on the moduli space) is invariant under permutations of the specified order of the side lengths. This invariance makes the homeomorphisms induced by these permutations into isometries. For cyclic permutations this invariance makes the geometry consistent with the perspective that the moduli space is a space of shapes, independent of the position and orientation of the shapes.

5.1 The Riemannian Metric

Recall from Definition 2.1.1 that

$$\mathcal{PM}(\vec{\ell}) = \left\{ (\mathbf{x}_1, \mathbf{x}_2, \mathbf{x}_3, \mathbf{x}_4) \in \mathbb{R}^8 : \|\mathbf{x}_i\| = \ell_i \text{ for all } i, \text{ and } \sum_{i=1}^{4} \mathbf{x}_i = \mathbf{0} \right\}$$

is a subset of $\mathbb{R}^8$.

The condition $\sum_{i=1}^{4} \mathbf{x}_i = \mathbf{0}$ imposed on $\mathcal{PM}(\vec{\ell})$ means that we can write the longest vector as a linear combination of the shorter three vectors. For ease of notation, and without loss of generality, we will assume that $\mathbf{x}_4$ is the longest vector. Then we can write $\mathbf{x}_4 = -\mathbf{x}_1 - \mathbf{x}_2 - \mathbf{x}_3$. Thus we can alternatively define $\mathcal{PM}(\vec{\ell})$ as

$$\mathcal{PM}(\vec{\ell}) = \left\{ (\mathbf{x}_1, \mathbf{x}_2, \mathbf{x}_3, \mathbf{x}_4) \in \mathbb{R}^8 : \|\mathbf{x}_i\| = \ell_i \text{ for all } i, \text{ and } \mathbf{x}_4 = -\sum_{i=1}^{3} \mathbf{x}_i \right\} \tag{5.1}$$

There is a natural embedding of $\mathcal{PM}(\vec{\ell})$ into $\mathbb{R}^6$ given by the projection map onto the shortest three vectors:

$$(\mathbf{x}_1, \mathbf{x}_2, \mathbf{x}_3, -\mathbf{x}_1 - \mathbf{x}_2 - \mathbf{x}_3) \longmapsto (\mathbf{x}_1, \mathbf{x}_2, \mathbf{x}_3)$$

Thus a point in $\mathcal{PM}(\vec{\ell})$ can be represented by the shortest three vectors, $(\mathbf{x}_1, \mathbf{x}_2, \mathbf{x}_3)$. We will work in the context of $\mathcal{PM}(\vec{\ell}) \subset \mathbb{R}^6$ for the remainder of the chapter.

Because we can view $\mathcal{PM}(\vec{\ell})$ as a surface in $\mathbb{R}^6$, $\mathcal{PM}(\vec{\ell})$ has the Riemannian metric induced by the Euclidean metric in $\mathbb{R}^6$: that is, the traditional dot product in $\mathbb{R}^6$ applied to the tangent vectors of $\mathcal{PM}(\vec{\ell})$ [9]. Because the metric on $\mathbb{R}^6$ is invariant under rigid rotations, the metric on $\mathcal{PM}(\vec{\ell})$ is invariant under the $SO(2)$ action on $\mathcal{PM}(\vec{\ell})$.

Recall that $\mathcal{PM}(\vec{\ell})$ is a 2-manifold everywhere but at the straight-line configurations. For the rest of this chapter we assume that $\vec{\ell}$ admits no straight-line configurations, and thus $\mathcal{PM}(\vec{\ell})$ is a smooth 2-manifold. Note that this assumption implies that $\mathcal{PM}(\vec{\ell})$ is homeomorphic to either one or two disjoint tori.

It is useful to parametrize $\mathcal{PM}(\vec{\ell})$ with local coordinates (u, v) and define the metric in terms of these coordinates.

Definition 5.1.1. Let $f : \mathbb{R}^2 \longrightarrow \mathcal{PM}(\vec{\ell})$ be given by

$$f(u,v) =$$

$$(\ell_1 \cos(\Phi_1(u,v)), \ell_1 \sin(\Phi_1(u,v)), \ell_2 \cos(\Phi_2(u,v)), \ell_2 \sin(\Phi_2(u,v)), \ell_3 \cos(\Phi_3(u,v)), \ell_3 \sin(\Phi_3(u,v)))$$

$$= (x_1, y_1, x_2, y_2, x_3, y_3)$$

where Φ_i is the angle of vector $\mathbf{x}_i = (x_i, y_i)$.

Then the inner product on tangent vectors of $\mathcal{PM}(\vec{\ell})$ is the pullback of the inner product

on $\mathbb{R}^6$:

$$f^*\left(\sum_{i=1}^{3} dx_i \otimes dx_i + dy_i \otimes dy_i\right)$$

where the expression of $f^*(dx_i \otimes dx_i)$ in (u, v)-coordinates is:

$$\begin{aligned} f^*(dx_i \otimes dx_i) &= ((x_i)_u du + (x_i)_v dv) \otimes ((x_i)_u du + (x_i)_v dv) \\ &= (x_i)_u^2 du \otimes du + (x_i)_u (x_i)_v dv \otimes du + (x_i)_u (x_i)_v du \otimes dv + (x_i)_v^2 dv \otimes dv \end{aligned}$$

and similarly for $f^*(dy_i \otimes dy_i)$.

This inner product on the tangent vectors of $\mathcal{PM}(\vec{\ell})$ has a matrix representation: Let k_{11} be the coefficient of $du \otimes du$, k_{12} be the coefficient of $du \otimes dv$ and $dv \otimes du$, and k_{22} be the coefficient of $dv \otimes dv$. If $\mathbf{a}, \mathbf{b} \in \mathbb{R}^2$ are the expressions in (u, v)-coordinates of vectors associated with vectors in $T_P(\mathcal{PM})$ by the Jacobian of f, where $T_P(\mathcal{PM})$ is the tangent space to $\mathcal{PM}(\vec{\ell})$ at a point $P \in \mathcal{PM}(\vec{\ell})$, then

$$< \mathbf{a}, \mathbf{b} >= \mathbf{a}^T \begin{pmatrix} k_{11} & k_{12} \\ k_{12} & k_{22} \end{pmatrix} \mathbf{b}$$

5.2 Local Coordinates for $\mathcal{PM}(\vec{\ell})$

We now choose specific local coordinates, (u, v), that are convenient for parametrizing $\mathcal{PM}(\vec{\ell})$. Let v be the angle of vector $-\mathbf{x}_4$ and u be one of the following (depending on the point in $\mathcal{PM}(\vec{\ell})$ around which the local coordinates are defined):

1. u_1: the angle measured counterclockwise from $-\mathbf{x}_4$ to $\mathbf{x}_1$

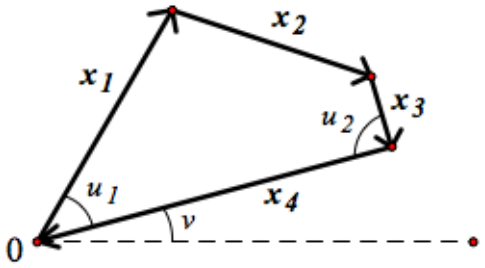

Figure 5.1: The angle v and the two choices for angle u: u_1 or u_2.

2. u_2: the angle measured counterclockwise from $-\mathbf{x}_3$ to $\mathbf{x}_4$

as shown in Figure 5.1. The angle u determines the shape of the quadrilateral (locally) and the angle v represents its position along the $SO(2)$-orbit in $\mathcal{PM}(\vec{\ell})$. Fixing u and changing v is equivalent to a rigid rotation of all the vector sides. Note that the paths described on $\mathcal{M}(\vec{\ell})$ in Chapter 4 could be viewed as paths in $\mathcal{PM}(\vec{\ell})$ with $v = 0$.

We think of changing v as motion in the "vertical" direction (along the $SO(2)$-orbits) in $\mathcal{PM}(\vec{\ell})$. Vertical motion in $\mathcal{PM}(\vec{\ell})$ leaves you fixed in $\mathcal{M}(\vec{\ell})$. Therefore the motion in $\mathcal{PM}(\vec{\ell})$ which best represents motion in $\mathcal{M}(\vec{\ell})$ will be in the direction orthogonal to vertical motion. We call this the "horizontal" direction.

With the coordinates ordered as (u, v), horizontal motion will be motion in the direction of the tangent vector, (a, b), that satisfies the following equation:

$$\begin{aligned}(a,b)\begin{pmatrix} k_{11} & k_{12} \\ k_{12} & k_{22}\end{pmatrix}\begin{pmatrix}0\\1\end{pmatrix} &= 0\\ k_{12}a + k_{22}b &= 0\\ \frac{b}{a} &= -\frac{k_{12}}{k_{22}}\end{aligned}$$

Proposition 5.2.1. *If v is the angle chosen above, then $k_{22} = \sum_{i=1}^{3}(x_i)_v^2 + (y_i)_v^2$ is a positive constant.*

Proof. Let $\mathbf{x}_i = (\ell_i \cos(\Phi_i), \ell_i \sin(\Phi_i))$ be the side vectors for $i = 1, 2, 3$. If v is the angle of -$\mathbf{x}_4$, then motion in the vertical direction is simply adding v to angles of each vector: $\mathbf{x}_i = (\ell_i \cos(\Phi_i + v), \ell_i \sin(\Phi_i + v))$ for $i = 1, 2, 3$.

Then $(\mathbf{x}_i)_v = (-\ell_i \sin(\Phi_i + v), \ell_i \cos(\Phi_i + v)) = ((x_i)_v, (y_i)_v)$, and

$$\begin{aligned}k_{22} &= \sum_{i=1}^{3}(x_i)_v^2 + (y_i)_v^2\\ &= \ell_1^2 + \ell_2^2 + \ell_3^2\\ &> 0\end{aligned}$$

□

Although k_{22} is constant, $k_{12} = \sum_{i=1}^{3}(x_i)_u(x_i)_v + (y_i)_u(y_i)_v$ depends on both u and v.

There is an induced slope field, $(k_{22}, -k_{12})$, at each point of $\mathcal{PM}(\vec{\ell})$. We desire a function $v = f(u)$ such that $\frac{df}{du} = -\frac{k_{12}}{k_{22}}$ because the graph of this function will define a horizontal

path.

Proposition 5.2.2. *For a fixed u, $-\dfrac{k_{12}(u,v)}{k_{22}}$ is independent of v.*

Proof. Let $(u,v),(\widetilde{u},\widetilde{v}) \in \mathcal{PM}(\vec{\ell})$ lie in the same vertical fiber. In other words, suppose $u = \widetilde{u}$ and $\widetilde{v} = v + v_0$, where v_0 is some fixed angle between zero and 2π. Since we have already shown that k_{22} is constant, it suffices to show that $k_{12}(\widetilde{u},\widetilde{v}) = k_{12}(u,v)$. Note that for all i,

$$\mathbf{x}_i = \begin{pmatrix} x_i(\widetilde{u},\widetilde{v}) \\ \\ y_i(\widetilde{u},\widetilde{v}) \end{pmatrix} = \begin{pmatrix} \cos(v_0) & -\sin(v_0) \\ \\ \sin(v_0) & \cos(v_0) \end{pmatrix} \begin{pmatrix} x_i(u,v) \\ \\ y_i(u,v) \end{pmatrix}$$

Therefore for all i,

$$\begin{aligned} x_i(\widetilde{u},\widetilde{v}) &= \cos(v_0)x_i(u,v) - \sin(v_0)y_i(u,v) \\ y_i(\widetilde{u},\widetilde{v}) &= \sin(v_0)x_i(u,v) + \cos(v_0)y_i(u,v) \end{aligned}$$

By definition,

$$k_{12}(\widetilde{u},\widetilde{v}) = \sum_{i=1}^{3} \frac{\partial x_i}{\partial \widetilde{u}}\frac{\partial x_i}{\partial \widetilde{v}} + \frac{\partial y_i}{\partial \widetilde{u}}\frac{\partial y_i}{\partial \widetilde{v}}$$

Since $\dfrac{du}{d\widetilde{u}} = 1$ and $\dfrac{dv}{d\widetilde{v}} = 1$, for all i,

$$\begin{aligned} \frac{\partial x_i}{\partial \widetilde{u}} &= \cos(v_0)\frac{\partial x_i}{\partial u}\frac{du}{d\widetilde{u}} - \sin(v_0)\frac{\partial y_i}{\partial u}\frac{du}{d\widetilde{u}} \\ &= \cos(v_0)\frac{\partial x_i}{\partial u} - \sin(v_0)\frac{\partial y_i}{\partial u} \\ \frac{\partial x_i}{\partial \widetilde{v}} &= \cos(v_0)\frac{\partial x_i}{\partial v} - \sin(v_0)\frac{\partial y_i}{\partial v} \end{aligned}$$

Similarly, for all i,

$$\begin{aligned}\frac{\partial y_i}{\partial \widetilde{u}} &= \sin(v_0)\frac{\partial x_i}{\partial u} + \cos(v_0)\frac{\partial y_i}{\partial u} \\ \frac{\partial y_i}{\partial \widetilde{v}} &= \sin(v_0)\frac{\partial x_i}{\partial v} + \cos(v_0)\frac{\partial y_i}{\partial v}\end{aligned}$$

Then for all i,

$$\begin{aligned}\frac{\partial x_i}{\partial \widetilde{u}}\frac{\partial x_i}{\partial \widetilde{v}} &= \left(\cos(v_0)\frac{\partial x_i}{\partial u} - \sin(v_0)\frac{\partial y_i}{\partial u}\right)\left(\cos(v_0)\frac{\partial x_i}{\partial v} - \sin(v_0)\frac{\partial y_i}{\partial v}\right) \\ &= \cos^2(v_0)\frac{\partial x_i}{\partial u}\frac{\partial x_i}{\partial v} - \cos(v_0)\sin(v_0)\frac{\partial x_i}{\partial v}\frac{\partial y_i}{\partial u} + \sin^2(v_0)\frac{\partial y_i}{\partial u}\frac{\partial y_i}{\partial v} - \cos(v_0)\sin(v_0)\frac{\partial x_i}{\partial u}\frac{\partial y_i}{\partial v}\end{aligned}$$

and

$$\begin{aligned}\frac{\partial y_i}{\partial \widetilde{u}}\frac{\partial y_i}{\partial \widetilde{v}} &= \left(\sin(v_0)\frac{\partial x_i}{\partial u} + \cos(v_0)\frac{\partial y_i}{\partial u}\right)\left(\sin(v_0)\frac{\partial x_i}{\partial v} + \cos(v_0)\frac{\partial y_i}{\partial v}\right) \\ &= \sin^2(v_0)\frac{\partial x_i}{\partial u}\frac{\partial x_i}{\partial v} + \cos(v_0)\sin(v_0)\frac{\partial x_i}{\partial v}\frac{\partial y_i}{\partial u} + \cos^2(v_0)\frac{\partial y_i}{\partial u}\frac{\partial y_i}{\partial v} + \cos(v_0)\sin(v_0)\frac{\partial x_i}{\partial u}\frac{\partial y_i}{\partial v}\end{aligned}$$

Then observe for all i,

$$\frac{\partial x_i}{\partial \widetilde{u}}\frac{\partial x_i}{\partial \widetilde{v}} + \frac{\partial y_i}{\partial \widetilde{u}}\frac{\partial y_i}{\partial \widetilde{v}} = \frac{\partial x_i}{\partial u}\frac{\partial x_i}{\partial v} + \frac{\partial y_i}{\partial u}\frac{\partial y_i}{\partial v}$$

Therefore,

$$\begin{aligned}k_{12}(\widetilde{u},\widetilde{v}) &= \sum_{i=1}^{3}\frac{\partial x_i}{\partial \widetilde{u}}\frac{\partial x_i}{\partial \widetilde{v}} + \frac{\partial y_i}{\partial \widetilde{u}}\frac{\partial y_i}{\partial \widetilde{v}} \\ &= \sum_{i=1}^{3}\frac{\partial x_i}{\partial u}\frac{\partial x_i}{\partial v} + \frac{\partial y_i}{\partial u}\frac{\partial y_i}{\partial v} \\ &= k_{12}(u,v)\end{aligned}$$

□

5.3 Paths in Spaces of Planar Quadrilaterals

5.3.1 Single Covering Paths in $\mathcal{M}(\vec{\ell})$

Definition 5.3.1. Let $X \in \mathcal{M}(\vec{\ell})$. Let $\gamma : [0,1] \longrightarrow \mathcal{M}(\vec{\ell})$ be a path satisfying:

1. $\gamma(0) = \gamma(1) = X$, and
2. γ makes exactly one full trip around the component of $\mathcal{M}(\vec{\ell})$ in which X lies.

Then γ is called a *single covering path of* $\mathcal{M}(\vec{\ell})$.

Note that the starting and ending point, X, is arbitrary. The path γ begins and ends at the same point in $\mathcal{M}(\vec{\ell})$, but passes exactly once through all other points in the component of $\mathcal{M}(\vec{\ell})$ in which X lies. We now prove some properties of single covering paths.

Let $A \geq B \geq C \geq D$ be the side lengths of $\vec{\ell}$ arranged in non-ascending order. Let $\mathbf{x}_A$ be the vector side with length A and let $\mathbf{x}_B, \mathbf{x}_C, \mathbf{x}_D$ be defined similarly. Let θ_A be the angle of vector $\mathbf{x}_A$ and let $\theta_B, \theta_C, \theta_D$ be defined similarly. Recall that

$$\mathbf{x}_A + \mathbf{x}_B + \mathbf{x}_C + \mathbf{x}_D = \mathbf{0} \tag{5.2}$$

at all points in γ.

Lemma 5.3.2. *Let $\vec{\ell}$ be such that $\mathcal{M}(\vec{\ell})$ is in Case (b) or Case (c) (refer back to Section 3.3). Let γ be a single covering path of one component of $\mathcal{M}(\vec{\ell})$. Then at every point in γ, $\theta_B \neq \theta_A$ and $\theta_C \neq \theta_A$.*

Proof. We will give a proof by contradiction. First suppose that, for some point in γ, $\theta_B = \theta_A$ and therefore $\mathbf{x}_A$ and $\mathbf{x}_B$ point in the same direction. By Equation (5.2) we must also have $\mathbf{x}_A + \mathbf{x}_B = -(\mathbf{x}_C + \mathbf{x}_D)$. This can happen if and only if $A + B < C + D$, which is true if and only if $A - D < C - B$. But $A - D \geq 0$ and $C - B \leq 0$, so this is a contradiction. (Note: by assuming that $\mathcal{M}(\vec{\ell})$ is in Case (b) or (c) we cannot have $A + B = C + D$).

Now suppose that for some point in γ, $\theta_C = \theta_A$ and therefore $\mathbf{x}_A$ and $\mathbf{x}_C$ point in the same direction. By Equation (5.2) we must also have $\mathbf{x}_A + \mathbf{x}_C = -(\mathbf{x}_B + \mathbf{x}_D)$. This can happen if and only if $A + C < B + D$ which is true if and only if $A - D < B - C$. But this is a contradiction to the assumption $A \geq B \geq C \geq D$.

□

Lemma 5.3.3. *If $\mathcal{M}(\vec{\ell})$ is in Case (b), then $\theta_D \neq \theta_A$ for every point in γ.*

Proof. Again we will give a proof by contradiction. Suppose that for some point in γ, $\theta_D = \theta_A$ and therefore $\mathbf{x}_A$ and $\mathbf{x}_D$ point in the same direction. By Equation (5.2) we must also have $\mathbf{x}_A + \mathbf{x}_D = -(\mathbf{x}_B + \mathbf{x}_C)$. This can happen if and only if $A + D < B + C$. But this is a contradiction to the connectedness condition given in Theorem 3.2.7, and since we are in Case (b), the moduli space $\mathcal{M}(\vec{\ell})$ is connected.

□

Now we will show that, if $\mathcal{M}(\vec{\ell})$ is in Case (c), γ is a single covering path of one component of $\mathcal{M}(\vec{\ell})$, and $\mathbf{x}_A$ is fixed in some direction, then $\mathbf{x}_D$ makes a full revolution on γ.

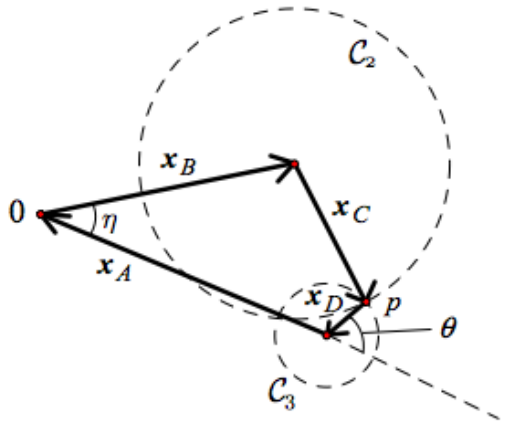

Figure 5.2: The angles η and θ.

First we define some angles we will use in the proof. Let η be the angle measured counterclockwise from -$\mathbf{x}_A$ to $\mathbf{x}_B$ and let θ be the angle measured counterclockwise from -$\mathbf{x}_A$ to -$\mathbf{x}_D$ (see Figure 5.2). Also recall that $\mathcal{C}_2$ is the circle with center $\mathbf{x}_B$ and radius C, and $\mathcal{C}_3$ is the circle with center -$\mathbf{x}_A$ and radius D (again, see Figure 5.2).

Theorem 5.3.4. *Let $\mathcal{M}(\vec{\ell})$ be in Case (c) and let γ be a single covering path of one component of $\mathcal{M}(\vec{\ell})$. Then θ realizes every angle in $[0, 2\pi]/0 \sim 2\pi$ exactly once on γ. Therefore if $\mathbf{x}_A$ is fixed in some direction, $\mathbf{x}_D$ makes one full revolution.*

Proof. We will show there exists a continuous map $h : \mathcal{M}(\vec{\ell}) \longrightarrow [0, 2\pi]/0 \sim 2\pi$ where h's values are θ. We will then show that the restriction of h to one component of $\mathcal{M}(\vec{\ell})$ is one-to-one and onto. Then because h maps a compact set to a compact set, the restriction of h must have a continuous inverse from $[0, 2\pi]/0 \sim 2\pi$ to that component of $\mathcal{M}(\vec{\ell})$. Hence the restriction of h is a homeomorphism.

Let $\mathcal{M}_1 \subset \mathcal{M}(\vec{\ell})$ be the component of $\mathcal{M}(\vec{\ell})$ that γ covers, i.e., let $\gamma : [0,1] \longrightarrow \mathcal{M}_1$ be a single covering path. Without loss of generality, assume that $\mathcal{M}_1$ is the component of $\mathcal{M}(\vec{\ell})$ in which $\mathbf{x}_B$ remains "above" the line in the plane passing through $\mathbf{x}_A$ (e.g., if $\mathbf{x}_A$ is fixed along the x-axis then $\mathcal{M}_1$ is the component of $\mathcal{M}(\vec{\ell})$ in which $\mathbf{x}_B$ remains above the x-axis). Let $h|_{\mathcal{M}_1}$ be the restriction of h to $\mathcal{M}_1$. Once we show that $h|_{\mathcal{M}_1}$ is a homeomorphism from $\mathcal{M}_1$ to $[0,2\pi]/0 \sim 2\pi$ we will have a continuous, onto, one-to-one path, $h|_{\mathcal{M}_1}(\gamma(t)) : [0,1] \longrightarrow [0,2\pi]/0 \sim 2\pi$, hence θ realizes every angle in $[0,2\pi]/0 \sim 2\pi$ exactly once on γ.

Observe that if $\mathbf{x}_A$ is fixed in some direction then θ and θ_D differ by a constant. Hence if θ realizes every angle in $[0,2\pi]/0 \sim 2\pi$ exactly once on γ then θ_D also realizes every angle in $[0,2\pi]/0 \sim 2\pi$ exactly once on γ. Therefore, if $\mathbf{x}_A$ is fixed in some direction, then $\mathbf{x}_D$ makes one full revolution.

First we show that h is continuous:

Fix $\theta_A = \pi$ (so that $\mathbf{x}_A$ lies on the x-axis) and let $m = (a,b,c,d) \in \mathcal{M}(\vec{\ell})$ be a point in the moduli space (see Figure 5.3). Observe that (a,b) depends continuously on η by an explicit formula, (c,d) can be written as a function of (a,b) everywhere but at isolated points (but has a continuous extension to those points, see the proof of Lemma 3.2.4), and θ depends continuously on (c,d) by appropriate branches of arccos and arcsin. Hence θ depends continuously on η for paths that do not pass through the isolated points (which are the points where $\mathbf{x}_C$ and $\mathbf{x}_D$ are parallel). For paths that do pass through these points, the intervals of θ's continuous dependence on η patch together at the endpoints to make θ depend continuously on points in $\mathcal{M}(\vec{\ell})$.

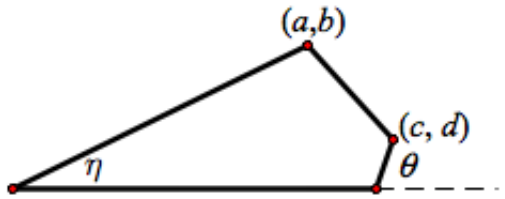

Figure 5.3: A point $m = (a, b, c, d)$ in the moduli space $\mathcal{M}(\vec{\ell})$.

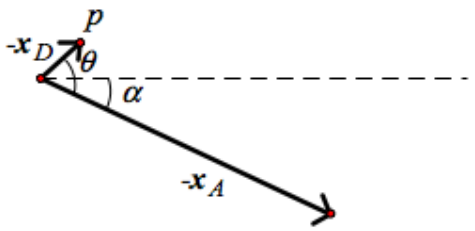

Figure 5.4: The point p's angle with the horizontal is $\theta - \alpha$.

Next we show that $h|_{\mathcal{M}_1}$ is onto:

Let $p = \mathbf{x}_B + \mathbf{x}_C = -(\mathbf{x}_A + \mathbf{x}_D)$. Then θ is the angle p makes with the line extending in the direction of $-\mathbf{x}_A$. Let α be the angle measured counterclockwise from $-\mathbf{x}_A$ to the horizontal. Then the angle p makes with the horizontal is equal to $\theta - \alpha$ (see Figure 5.4) and $p = (A\cos(\alpha), -A\sin(\alpha)) + (D\cos(\theta-\alpha), D\sin(\theta-\alpha))$. If we fix θ, fix $\mathbf{x}_B$, and increase η by moving $\mathbf{x}_A$, then p as a point in the plane depends continuously on η as revealed by the above formula and the observation that, if θ_B is fixed, then η and α differ by a constant (which we call θ_B).

Let $\theta \in [0, 2\pi]/0 \sim 2\pi$. Then θ corresponds to a point p on the circle $\mathcal{C}_3$. If p also lies on circle $\mathcal{C}_2$ (i.e., is an intersection point of $\mathcal{C}_2$ and $\mathcal{C}_3$), then there is a point $m \in \mathcal{M}(\vec{\ell})$ such

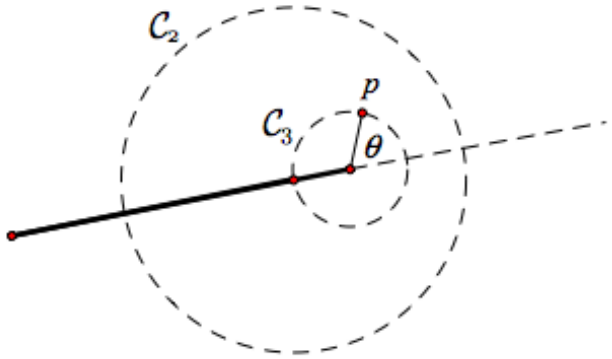

Figure 5.5: When $\eta = 0$, the circle $\mathcal{C}_3$ lies inside the disk bounded by circle $\mathcal{C}_2$.

that $h(m) = \theta$. We will now exhibit a path where, for a fixed θ, the corresponding point p begins inside the disk bounded by $\mathcal{C}_2$ and ends outside the disk bounded by $\mathcal{C}_2$. Then by the Intermediate Value Theorem there must be a place on the path where p lies on both $\mathcal{C}_2$ and $\mathcal{C}_3$.

Begin with $\eta = 0$ as shown in Figure 5.5. Because we are in Case (c) we have $A+D < B+C$. Therefore every point on $\mathcal{C}_3$ is completely contained in the disk bounded by $\mathcal{C}_2$ when $\eta = 0$.

Keeping $\mathbf{x}_B$ (and hence $\mathcal{C}_2$) fixed, increase η by moving $\mathbf{x}_A$. There exists some η_0 where $\mathcal{C}_2$ and $\mathcal{C}_3$ intersect with $\mathcal{C}_3$ still completely contained inside the disk bounded by $\mathcal{C}_2$ (excluding the point of intersection), see Figure 5.6. Let $p_0 \in \mathcal{C}_3$ be the point of intersection.

As η continues to increase from η_0 continuously there will be two points of intersection of $\mathcal{C}_2$ and $\mathcal{C}_3$. Eventually there will be some angle η_1 where $\mathcal{C}_2$ and $\mathcal{C}_3$ again intersect in only one point, call it p_1, but now the circle $\mathcal{C}_3$ lies completely outside the disk bounded by $\mathcal{C}_2$ (except for the point of intersection), see Figure 5.7.

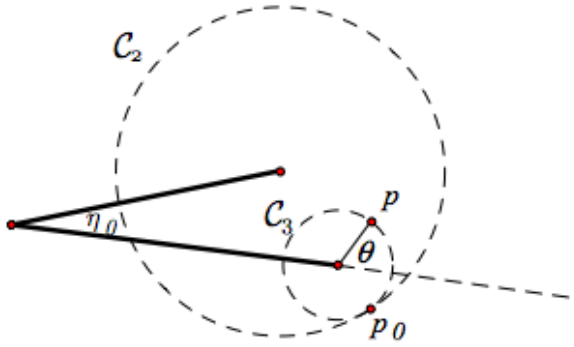

Figure 5.6: At η_0 there is one point of intersection of circles $\mathcal{C}_2$ and $\mathcal{C}_3$, named p_0.

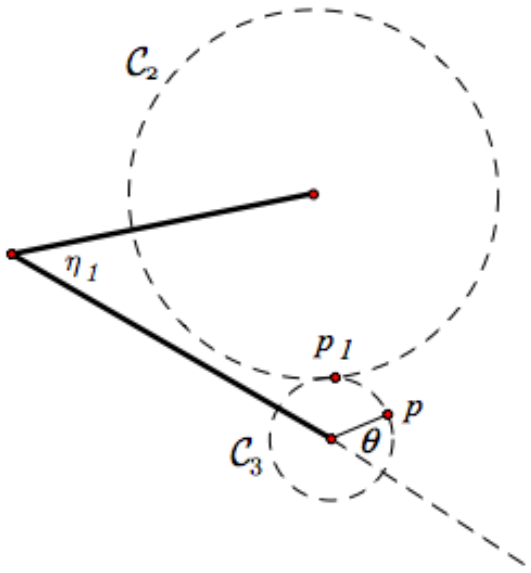

Figure 5.7: At η_1 there is one point of intersection of circles $\mathcal{C}_2$ and $\mathcal{C}_3$, named p_1.

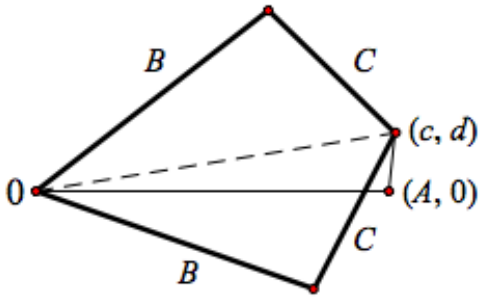

Figure 5.8: For a fixed (c, d) there are two possible triangles having sides $< c, d >$, $\mathbf{x}_B$ and $\mathbf{x}_C$.

Thus all points $p \neq p_1$ begin inside the disk bounded by $\mathcal{C}_2$ and end outside the disk bounded by $\mathcal{C}_2$ traveling along a path parametrized by η. Therefore every point on $\mathcal{C}_3$ intersects with $\mathcal{C}_2$ somewhere on that path and hence $h|_{\mathcal{M}_1}$ is onto. Observe that an analogous argument could be made for $h|_{\mathcal{M}_2}$ onto, where $\mathcal{M}_2$ is the other component of $\mathcal{M}(\vec{\ell})$.

Now we show that $h|_{\mathcal{M}_1}$ is one-to-one:

Fix (c, d). Then the three vectors $< c, d >, \mathbf{x}_B$, and $\mathbf{x}_C$ form two possible triangles, each triangle associated with a unique point in $\mathcal{M}(\vec{\ell})$ (see Figure 5.8). By the proof of $h|_{\mathcal{M}_1}$ and $h|_{\mathcal{M}_2}$ being onto, for each component in $\mathcal{M}(\vec{\ell})$ there must be a unique point associated with such a triangle. Therefore in one component of $\mathcal{M}(\vec{\ell})$ there is only one point that can map to (c, d). Therefore h is one-to-one on each component.

□

5.3.2 Horizontal Lifts of Single Covering Paths

Recall that $\pi : \mathcal{PM}(\vec{\ell}) \longrightarrow \mathcal{M}(\vec{\ell})$ is the quotient map.

Definition 5.3.5. Let $\gamma : [0,1] \longrightarrow \mathcal{M}(\vec{\ell})$ be a single covering path in the moduli space. Define the *horizontal lift of* γ to be $\widetilde{\gamma} : [0,1] \longrightarrow \mathcal{PM}(\vec{\ell})$ by $\widetilde{\gamma}(t) = (t, v(t))$ such that $\widetilde{\gamma}$ satisfies:

1. $\pi(\widetilde{\gamma}(t)) = \gamma(t)$, and
2. $\widetilde{\gamma}'(t) = \left(1, -\dfrac{k_{12}}{k_{22}}\right)$

Note that $\widetilde{\gamma}$ remains in one of the components of $\mathcal{PM}(\vec{\ell})$, which is a torus. We must have $\widetilde{\gamma}(0), \widetilde{\gamma}(1) \in \pi^{-1}(X)$. A natural question that arises is whether $\widetilde{\gamma}(0) = \widetilde{\gamma}(1)$. We wish to calculate the total accumulated change in the v-direction as $\widetilde{\gamma}$ follows the induced slope field in the horizontal direction on $\mathcal{PM}(\vec{\ell})$. If that total accumulated change is equal to zero or an integer multiple of 2π, then we must have $\widetilde{\gamma}(0) = \widetilde{\gamma}(1)$. Otherwise, $\widetilde{\gamma}(0) \neq \widetilde{\gamma}(1)$ and we have holonomy.

If we wish to calculate the total accumulated change in v, we can use the following integral with $\dfrac{dv}{du}$ expressed in local coordinates:

$$\int_{\widetilde{\gamma}} dv = \int \frac{dv}{du}\,(u,v)\; du$$

Because k_{22} is constant and $\dfrac{dv}{du}\,(u_0, v)$ is independent of v for each u_0, we may do our

calculations with $v = 0$:

$$\begin{aligned} \int_{\widetilde{\gamma}} dv &= \int -\frac{k_{12}}{k_{22}}(u,v)\, du \\ &= -\frac{1}{k_{22}} \int k_{12}(u,0)\, du \end{aligned}$$

Recall that we assume $\ell_4 = A$ is the longest side. Doing calculations with $v = 0$ then becomes equivalent to doing calculations with $\theta_A = \pi$.

Lemma 5.3.6. *Let $\mathcal{M}(\vec{\ell})$ be in Case (b). Then for all i the net change in $\mathbf{x}_i$'s angle around γ is zero.*

Proof. Let θ_i be $\mathbf{x}_i$'s angle for all i. Recall that $\theta_4 = \pi$ is fixed. By definition of γ, each vector $\mathbf{x}_i$ begins and ends at the same angle. Therefore θ_i's net change around γ is either zero or an integer multiple of 2π. Clearly θ_4's net change is zero since $\mathbf{x}_4$ remains fixed. To show that θ_i's net change around γ is zero for $i = 1, 2, 3$ it suffices to show that $\theta_i \neq \pi$ for $i = 1, 2, 3$. Since $\mathcal{M}(\vec{\ell})$ is in Case (b), Lemmas 5.3.2 and 5.3.3 show that $\theta_i \neq \pi$ for $i = 1, 2, 3$.

□

Lemma 5.3.7. *Let $\mathcal{M}(\vec{\ell})$ be in Case (c). Then the net change in $\mathbf{x}_D$'s angle around γ is $\pm 2\pi$, but the net change in all other vector sides around γ is zero.*

Proof. Because $\theta_A = \pi$ is fixed, its net change around γ is clearly zero. Lemma 5.3.2 shows that $\theta_B \neq \pi$ and $\theta_C \neq \pi$ for all points in γ. Theorem 5.3.4 shows that $\mathbf{x}_D$'s net change around γ is $\pm 2\pi$. □

5.3.3 Theorem For Case (b)

Theorem 5.3.8. *If $\vec{\ell}$ is chosen such that $\mathcal{M}(\vec{\ell})$ is homeomorphic to $\mathcal{S}^1$ and γ is a single covering path of $\mathcal{M}(\vec{\ell})$, then for a horizontal lift $\widetilde{\gamma}$, $\int_{\widetilde{\gamma}} dv = 0$.*

Proof. Recall from Lemma 5.3.6 that for $i = 1, 2, 3$, the net change in $\mathbf{x}_i$'s angle around γ is zero.

$$\begin{aligned}\int_{\widetilde{\gamma}} dv &= -\frac{1}{k_{22}} \int k_{12}(u,0)\, du \\ &= -\frac{1}{k_{22}} \left(\sum_{i=1}^{3} \int \left(\frac{\partial \mathbf{x}_i}{\partial u} \cdot \frac{\partial \mathbf{x}_i}{\partial v} \right) du \right)\end{aligned}$$

We will show that $\int \frac{\partial \mathbf{x}_i}{\partial u} \cdot \frac{\partial \mathbf{x}_i}{\partial v}\, du = 0$ for all i. Then $\int_{\widetilde{\gamma}} dv = 0$.

1. For $i = 1$:

   Recall that $\mathbf{x}_1$'s angle is u when $v = 0$, except at isolated points. When $\mathbf{x}_1$'s angle is not u then it can still be written as a function of u and the Chain Rule may be applied, as will be shown below for $i = 2, 3$. Note that since $\mathbf{x}_1 = (\ell_1 \cos(u+v), \ell_1 \sin(u+v))$,

   $$\begin{aligned}\frac{\partial \mathbf{x}_1}{\partial u} &= \frac{\partial \mathbf{x}_1}{\partial v} \\ &= (-\ell_1 \sin(u+v), \ell_1 \cos(u+v))\end{aligned}$$

   Therefore,

   $$\frac{\partial \mathbf{x}_1}{\partial u} \cdot \frac{\partial \mathbf{x}_1}{\partial v} = \|(\mathbf{x}_1)_v\|^2 = \ell_1^2$$

   Around γ the net change in u is zero. Therefore

   $$\int \frac{\partial \mathbf{x}_1}{\partial u} \cdot \frac{\partial \mathbf{x}_1}{\partial v}\, du = \int \ell_1^2\, du = \ell_1^2(0) = 0$$

2. For $i = 2$:

   We have shown previously that we can write $c(a, b)$ and $d(a, b)$ everywhere except at isolated points, where $p_2 = (a, b)$ and $p_3 = (c, d)$. We also have $a(u) = \ell_1 \cos(u)$ and $b(u) = \ell_1 \sin(u)$. Let w be $\mathbf{x}_2$'s angle. Then

   $$(\ell_2 \cos(w), \ell_2 \sin(w)) = \mathbf{x}_2 = (c(u) - a(u), d(u) - b(u))$$

   Therefore we can define $w = f(u)$ on appropriate branches of arccos and arcsin.

   Because $dw = \dfrac{dw}{du} du$, by the Chain Rule,

   $$\begin{aligned} \int \frac{\partial \mathbf{x}_2}{\partial u} \cdot \frac{\partial \mathbf{x}_2}{\partial v} \, du &= \int \frac{\partial \mathbf{x}_2}{\partial w} \frac{dw}{du} \cdot \frac{\partial \mathbf{x}_2}{\partial v} \, du \\ &= \int \frac{\partial \mathbf{x}_2}{\partial w} \cdot \frac{\partial \mathbf{x}_2}{\partial v} \, dw \end{aligned}$$

   Because $\mathbf{x}_2 = (\ell_2 \cos(w + v), \ell_2 \sin(w + v))$, again we have that

   $$\begin{aligned} \frac{\partial \mathbf{x}_2}{\partial w} &= \frac{\partial \mathbf{x}_2}{\partial v} \\ &= (-\ell_2 \sin(w + v), \ell_2 \cos(w + v)) \end{aligned}$$

   And

   $$\frac{\partial \mathbf{x}_2}{\partial w} \cdot \frac{\partial \mathbf{x}_2}{\partial v} = \|(\mathbf{x}_2)_v\|^2 = \ell_2^2$$

   Around γ the net change in w is zero. Therefore

   $$\int \frac{\partial \mathbf{x}_2}{\partial w} \cdot \frac{\partial \mathbf{x}_2}{\partial v} \, dw = \int \ell_2^2 \, dw = \ell_2^2(0) = 0$$

3. For $i = 3$:

   Let z be $\mathbf{x}_3$'s angle. Then

   $$(\ell_3 \cos(z), \ell_3 \sin(z)) = \mathbf{x}_3 = (\ell_4 - c(u), -d(u))$$

Therefore we can define $z = f(u)$ on appropriate branches of arccos and arcsin.

Because $dz = \dfrac{dz}{du}du$, by the Chain Rule,

$$\begin{aligned}\int \frac{\partial \mathbf{x}_3}{\partial u} \cdot \frac{\partial \mathbf{x}_3}{\partial v}\, du &= \int \frac{\partial \mathbf{x}_3}{\partial z}\frac{dz}{du} \cdot \frac{\partial \mathbf{x}_3}{\partial v}\, du \\ &= \int \frac{\partial \mathbf{x}_3}{\partial z} \cdot \frac{\partial \mathbf{x}_3}{\partial v}\, dz\end{aligned}$$

Because $\mathbf{x}_3 = (\ell_3 \cos(z+v), \ell_3 \sin(z+v))$, again we have that

$$\begin{aligned}\frac{\partial \mathbf{x}_3}{\partial z} &= \frac{\partial \mathbf{x}_3}{\partial v} \\ &= (-\ell_3 \sin(z+v), \ell_3 \cos(z+v))\end{aligned}$$

And

$$\frac{\partial \mathbf{x}_3}{\partial z} \cdot \frac{\partial \mathbf{x}_3}{\partial v} = \|(\mathbf{x}_3)_v\|^2 = \ell_3^2$$

Around γ the net change in z is zero. Therefore

$$\int \frac{\partial \mathbf{x}_3}{\partial z} \cdot \frac{\partial \mathbf{x}_3}{\partial v}\, dz = \int \ell_3^2\, dz = \ell_3^2(0) = 0$$

□

5.3.4 Theorem For Case (c)

Theorem 5.3.9. *If $\vec{\ell}$ is chosen such that $\mathcal{M}(\vec{\ell})$ is homeomorphic to $\mathcal{S}^1 \sqcup \mathcal{S}^1$ and γ is a single covering path of one component of $\mathcal{M}(\vec{\ell})$ then, for a horizontal lift $\widetilde{\gamma}$, $\displaystyle\int_{\widetilde{\gamma}} dv = \pm\frac{2\pi\ell_3^2}{\ell_1^2+\ell_2^2+\ell_3^2}$, which is a nonzero value that is not an integer multiple of 2π. Therefore $\widetilde{\gamma}$ exhibits holonomy.*

Proof. Without loss of generality we may assume that $\mathbf{x}_B = \mathbf{x}_1, \mathbf{x}_C = \mathbf{x}_2$, and $\mathbf{x}_D = \mathbf{x}_3$. Then by Lemma 5.3.7 that the net change in $\mathbf{x}_1$ and $\mathbf{x}_2$'s angles around γ are both zero, but the net change in $\mathbf{x}_3$'s angle around γ is $\pm 2\pi$.

$$\begin{aligned}\int_{\widetilde{\gamma}} dv &= -\frac{1}{k_{22}} \int k_{12}(u,0)\, du \\ &= -\frac{1}{k_{22}} \left(\sum_{i=1}^{3} \int \left(\frac{\partial \mathbf{x}_i}{\partial u} \cdot \frac{\partial \mathbf{x}_i}{\partial v} \right) du \right)\end{aligned}$$

We will show that:

1. $\int \frac{\partial \mathbf{x}_1}{\partial u} \cdot \frac{\partial \mathbf{x}_1}{\partial v}\, du = 0$,
2. $\int \frac{\partial \mathbf{x}_2}{\partial u} \cdot \frac{\partial \mathbf{x}_2}{\partial v}\, du = 0$, and
3. $\int \frac{\partial \mathbf{x}_3}{\partial u} \cdot \frac{\partial \mathbf{x}_3}{\partial v}\, du = \pm \frac{2\pi \ell_3^2}{\ell_1^2 + \ell_2^2 + \ell_3^2}$.

Then $\int_{\widetilde{\gamma}} dv = \pm \frac{2\pi \ell_3^2}{\ell_1^2 + \ell_2^2 + \ell_3^2}$.

1. Recall that $\mathbf{x}_1$'s angle is u when $v = 0$, except at isolated points. When $\mathbf{x}_1$'s angle is not u then it can still be written as a function of u and the Chain Rule may be applied. Note that since $\mathbf{x}_1 = (\ell_1 \cos(u+v), \ell_1 \sin(u+v))$,

$$\begin{aligned}\frac{\partial \mathbf{x}_1}{\partial u} &= \frac{\partial \mathbf{x}_1}{\partial v} \\ &= (-\ell_1 \sin(u+v), \ell_1 \cos(u+v))\end{aligned}$$

Therefore,

$$\frac{\partial \mathbf{x}_1}{\partial u} \cdot \frac{\partial \mathbf{x}_1}{\partial v} = \|(\mathbf{x}_1)_v\|^2 = \ell_1^2$$

Around γ the net change in u is zero. Therefore

$$\int \frac{\partial \mathbf{x}_1}{\partial u} \cdot \frac{\partial \mathbf{x}_1}{\partial v}\, du = \int \ell_1^2\, du = \ell_1^2(0) = 0$$

2. We have shown previously that we can write $c(a,b)$ and $d(a,b)$ everywhere except at isolated points, where $p_2 = (a,b)$ and $p_3 = (c,d)$. We also have $a(u) = \ell_1 \cos(u)$ and $b(u) = \ell_1 \sin(u)$. Let w be $\mathbf{x}_2$'s angle. Then

$$(\ell_2 \cos(w), \ell_2 \sin(w)) = \mathbf{x}_2 = (c(u) - a(u), d(u) - b(u))$$

Therefore we can define $w = f(u)$ on appropriate branches of arccos and arcsin.

Because $dw = \dfrac{dw}{du} du$, by the Chain Rule,

$$\begin{aligned} \int \frac{\partial \mathbf{x}_2}{\partial u} \cdot \frac{\partial \mathbf{x}_2}{\partial v}\, du &= \int \frac{\partial \mathbf{x}_2}{\partial w} \frac{dw}{du} \cdot \frac{\partial \mathbf{x}_2}{\partial v}\, du \\ &= \int \frac{\partial \mathbf{x}_2}{\partial w} \cdot \frac{\partial \mathbf{x}_2}{\partial v}\, dw \end{aligned}$$

Because $\mathbf{x}_2 = (\ell_2 \cos(w+v), \ell_2 \sin(w+v))$, again we have that

$$\begin{aligned} \frac{\partial \mathbf{x}_2}{\partial w} &= \frac{\partial \mathbf{x}_2}{\partial v} \\ &= (-\ell_2 \sin(w+v), \ell_2 \cos(w+v)) \end{aligned}$$

And

$$\frac{\partial \mathbf{x}_2}{\partial w} \cdot \frac{\partial \mathbf{x}_2}{\partial v} = \|(\mathbf{x}_2)_v\|^2 = \ell_2^2$$

Around γ the net change in w is zero. Therefore

$$\int \frac{\partial \mathbf{x}_2}{\partial w} \cdot \frac{\partial \mathbf{x}_2}{\partial v}\, dw = \int \ell_2^2\, dw = \ell_2^2(0) = 0$$

3. Let z be $\mathbf{x}_3$'s angle. Then

$$(\ell_3 \cos(z), \ell_3 \sin(z)) = \mathbf{x}_3 = (\ell_4 - c(u), -d(u))$$

Therefore we can define $z = f(u)$ on appropriate branches of arccos and arcsin.

Because $dz = \dfrac{dz}{du} du$, by the Chain Rule,

$$\begin{aligned} \int \frac{\partial \mathbf{x}_3}{\partial u} \cdot \frac{\partial \mathbf{x}_3}{\partial v} \, du &= \int \frac{\partial \mathbf{x}_3}{\partial z} \frac{dz}{du} \cdot \frac{\partial \mathbf{x}_3}{\partial v} \, du \\ &= \int \frac{\partial \mathbf{x}_3}{\partial z} \cdot \frac{\partial \mathbf{x}_3}{\partial v} \, dz \end{aligned}$$

Because $\mathbf{x}_3 = (\ell_3 \cos(z + v), \ell_3 \sin(z + v))$, again we have that

$$\begin{aligned} \frac{\partial \mathbf{x}_3}{\partial z} &= \frac{\partial \mathbf{x}_3}{\partial v} \\ &= (-\ell_3 \sin(z + v), \ell_3 \cos(z + v)) \end{aligned}$$

And

$$\frac{\partial \mathbf{x}_3}{\partial z} \cdot \frac{\partial \mathbf{x}_3}{\partial v} = \|(\mathbf{x}_3)_v\|^2 = \ell_3^2$$

Around γ the net change in z is $\pm 2\pi$. Therefore

$$\int \frac{\partial \mathbf{x}_3}{\partial z} \cdot \frac{\partial \mathbf{x}_3}{\partial v} \, dz = \int \ell_3^2 \, dz = \ell_3^2(\pm 2\pi)$$

We have now shown that

$$\begin{aligned} \int_{\widetilde{\gamma}} dv &= \pm \frac{1}{k_{22}} (2\pi \ell_3^2) \\ &= \pm \frac{2\pi \ell_3^2}{\ell_1^2 + \ell_2^2 + \ell_3^2} \end{aligned}$$

Because $0 < \dfrac{\ell_3^2}{\ell_1^2+\ell_2^2+\ell_3^2} < 1$, $\pm\dfrac{2\pi\ell_3^2}{\ell_1^2+\ell_2^2+\ell_3^2}$ is never zero or an integer multiple of 2π. Therefore, in Case (c), $\widetilde{\gamma}(0) \neq \widetilde{\gamma}(1)$.

□

Chapter 6

Future Work

Some problems suggested by the present work appear below.

- Remark 4.3.2 states that we have not yet identified conditions on side lengths implying that it is always shorter to leave the plane when moving from $\mathcal{V}$ to $\mathcal{V}'$. Identification of these conditions and a proof of the result would tidy things up.

- If $\mathcal{M}(\vec{\ell})$ is homeomorphic to $\mathcal{S}^1$ then we can view a path between the two $\triangle$-configurations as a path from triangle to triangle that moves through quadrilaterals. A potentially interesting generalization of this would be examining paths from $\mathcal{V}$ to $\mathcal{V}'$ that move through pentagons, as would arise if one of the three robot arm segments has a flexible joint that is allowed to bend. Distances in spaces of pentagons seem not to have been studied, although the topology of moduli spaces of pentagons in the plane has already been completely classified [2].

- A triangle must always lie in a plane but a quadrilateral need not always lie in a plane. In $\mathbb{R}^3$ there are four-sided shapes that do not fit in a plane, and hence are not included in $\mathcal{M}(\vec{\ell})$. One could consider the moduli space of quadrilaterals in $\mathbb{R}^3$. The topology of the moduli space of quadrilaterals in $\mathbb{R}^3$ has not yet been studied. In $\mathbb{R}^2$ we viewed the moduli space as arising from intersections of circles; in $\mathbb{R}^3$ we can view the moduli space as arising from intersections of spheres. As the vectors whose endpoints are the centers of these spheres move closer together or farther apart, the moduli space in $\mathbb{R}^3$ is traced out by circles (because, in general, the intersection of two spheres is a circle). Our conjecture is that the moduli space of quadrilaterals in $\mathbb{R}^3$ is always homeomorphic to a sphere, even in the degenerate cases. There may be some interesting geometric properties of these spheres, particularly in the degenerate cases, but this has not been studied.

- The pre-moduli space of quadrilaterals in $\mathbb{R}^3$ has not yet been considered. Questions about holonomy in this pre-moduli space also arise. Because we expect the moduli space to always be homeomorphic to a sphere, all paths in the moduli space will be homotopic. If there is holonomy, it will arise from the curvature of the $SO(3)$ bundles over the moduli space.

- Complete classifications of the topology of the moduli space with $n > 5$ have not been studied.

Appendix A

Lemma 2.1.4 states:

There exists a map $H : \mathcal{M}(\vec{\ell}, n) \longrightarrow \mathcal{PM}(\vec{\ell}, n)$ *such that* $\pi(H(w)) = w$ *for all* $w \in \mathcal{M}(\vec{\ell}, n)$.

Proof. Let θ_k be the angle of vector side $\mathbf{x}_k$ for all $k = 1, \ldots, n$. We now identify points in $\mathbb{R}^2$ with points in $\mathbb{C}$: Let $g_k = \ell_k e^{i\theta_k} \in \mathbb{C}$ for $k = 1, \ldots, n$.

Claim: There exists $H : \mathcal{PM}(\vec{\ell}, n) \longrightarrow \mathcal{PM}(\vec{\ell}, n)$ such that $H(gw) = H(w)$ for all $g \in SO(2)$. Thus H defines a continuous section from $\mathcal{M}(\vec{\ell}, n)$ to $\mathcal{PM}(\vec{\ell}, n)$.

Define $H(g_1, \ldots, g_n) = (g_n^{-1} g_1, \ldots, g_n^{-1} g_n)$. The map $f(g_1, \ldots, g_n) = g_n^{-1}$ is continuous, and because

$$H(g_1, \ldots, g_n) = (f(g_1, \ldots, g_n) g_1, \ldots, f(g_1, \ldots, g_n) g_n)$$

is a composition of continuous functions, H is continuous.

Let elements in $SO(2)$ be identified with elements of $\mathbb{C}$ having modulus one. Let $g = e^{i\theta}$ be such an element. Let $w = (g_1, \ldots, g_n) \in \mathcal{PM}(\vec{\ell}, n)$.

Then $gw = (gg_1, \ldots, gg_n)$, $H(w) = (g_n^{-1}g_1, \ldots, g_n^{-1}g_n)$, and

$$\begin{aligned} H(gw) &= ((gg_n)^{-1}gg_1, \ldots, (gg_n)^{-1}gg_n) \\ &= (g_n^{-1}g^{-1}gg_1, \ldots, g_n^{-1}g^{-1}gg_n) \\ &= (g_n^{-1}g_1, \ldots, g_n^{-1}g_n) \\ &= H(w) \end{aligned}$$

□

Bibliography

[1] Glen E. Bredon, *Introduction to Compact Transformation Groups*, Academic Press (1972).

[2] Curtis, R. and M. Steiner, "Configuration Spaces of Planar Pentagons", *The American Mathematical Monthly* **114** (2007), 183—201.

[3] M. Farber, *Invitation to Topological Robotics*, European Mathematical Society (2008).

[4] R. V. Gamkrelidze (Ed.), *Geometry I*, Encyclopedia of Mathematical Sciences, Vol. 28, Springer-Verlag (1991).

[5] Kapovich, M. and J. Millson, "On The Moduli Space of Polygons in the Euclidean Plane", *J. Differential Geometry* **42(2)** (1995), 430—464.

[6] Kapovich, M. and J. J. Millson, "The Symplectic Geometry of Polygons in Euclidean Space", *J. Differential Geometry* **44** (1996), 479—513.

[7] D. G. Kendall et al., *Shape and Shape Theory*, Wiley (1999).

[8] Milgram, R. J. and J. C. Trinkle, "The Geometry of Configuration Spaces for Closed Chains in Two and Three Dimensions", *Homology, Homotopy and Applications* **6(1)** (2004), 237—267.

[9] B. O'Neill, *Elementary Differential Geometry,* 2^{nd} *Edition*, Academic Press (1997).

[10] Shimamoto, D. and C. Vanderwaart, "Spaces of Polygons in the Plane and Morse Theory", *The American Mathematical Monthly* **112** (2005), 289—310.